Polymersome Shape Transformation at the Nanoscale

ARTICLE *in* ACS NANO · SEPTEMBER 2013

Impact Factor: 12.88 · DOI: 10.1021/nn4039589 · Source: PubMed

Polymersomes Shape Transformation at the Nanoscale

Romain Salva,[†,‡] *Jean-François Le Meins,*[†] *Olivier Sandre,*[†] *Annie Brûlet,*[§] *Marc Schmutz,*[⊥] *Patrick Guenoun,*[*,‡] *and Sébastien Lecommandoux* [*,†]

[†]Université de Bordeaux/IPB, ENSCBP, 16 avenue Pey-Berland, 33607 Pessac, France, LCPO, UMR 5629, Pessac, France

[‡]IRAMIS, LIONS, UMR SIS2M 3299 CEA-CNRS, CEA Saclay, F-91191 Gif-sur-Yvette Cedex, France

[§]Laboratoire Léon Brillouin, LLB, UMR12, CNRS-CEA Saclay, F-91191 Gif-sur-Yvette Cedex, France

[⊥]Institut Charles Sadron, UPR 22 CNRS, Université de Strasbourg, 23 rue du Loess, 67034 Strasbourg, France

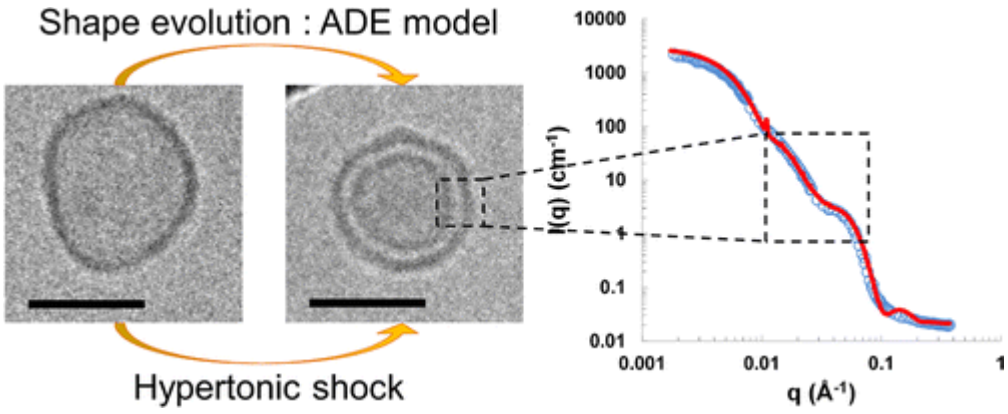

[*]Address correspondence to patrick.guenoun@cea.fr, lecommandoux@enscbp.fr.

ABSTRACT: Polymer vesicles, also named polymersomes, are valuable candidates for drug delivery and micro or nano-reactors applications. As far as drug delivery is concerned, the shape of the carrier is believed to have a strong influence on the biodistribution and cell internalization. Polymersomes can be submitted to an osmotic imbalance when injected in physiological media leading to morphological changes. To understand these osmotic stress-induced variations in membrane properties and shapes, several nano-vesicles made of the graft polymer poly(dimethylsiloxane)-*g*-poly(ethylene oxide) (PDMS-*g*-PEO) or the triblock copolymer PEO-*b*-PDMS-*b*-PEO were osmotically stressed and observed by light scattering, neutron scattering (SANS) and cryo-transmission electron microscopy (cryo-TEM). Hypotonic shock leads to a swelling of the vesicles, comparable to optically observable giant polymersomes, and hypertonic shock leads to collapsed structures such as stomatocytes and original nested vesicles *the latter being only observed for diblocks*. Complementary SANS and cryo-TEM experiments are shown to be in quantitative agreement and highlight the importance of the membrane structure on the behavior of these nano-polymersomes under hypertonic conditions as the final morphology reached depends whether or not the copolymers assemble into a bilayer. The vesicle radius and membrane curvature are also shown to be critical parameters for such transformations: the shape evolution trajectory agrees with theoretical models only for large enough vesicle radii above a threshold value around four times the membrane thickness.

KEYWORDS: block copolymer, vesicles, polymersomes, shape transformation, osmotic shock, bi-lamellar membrane, nested vesicles, permeability

Self-assembly of amphiphilic block copolymers in aqueous solution is a versatile and widely used method for the formation of nanostructures with various shapes. By structural analogy with viral capsids, polymeric vesicular structures (polymersomes)[1, 2] are under intense scrutiny for triggered release drug delivery[3, 4] but also for micro or nano-reactors applications.[5-7] Moreover, like lipidic vesicles (liposomes), polymersomes can be considered as a simplified model for living membranes and thus be used for basic cellular behavior studies.[8] Indeed membrane proteins have been successfully incorporated in polymersomes membranes[9, 10] and hierarchical self-assemblies mimicking the structure of cells have been reported.[11] In terms of mechanics, the membrane of polymersomes shows improved mechanical resistance as compared to liposomes. As a matter of fact, the polymeric membrane usually has a higher bending moduli and lysis strain, and a lower permeability to both solvent and solutes.[1, 12]

One of the next crucial steps for the future use of polymersomes consists in controlling their shape. In a biomimetic approach, the behavior of many cells in physiological environment is related to their shape and conformational changes can go along with severe diseases. As an example, human red blood cells (RBCs) form a biconcave discoid shape (discocyte) under healthy conditions but blood diseases such as malaria[13, 14] or drepanocytosis (formation of sickle shaped red blood cell) are related to changes in the RBCs shape. The interaction between cells and nanoparticles also depends on the shape of these latter. Indeed, in addition to nanoparticle's size that is obviously a relevant parameter,[15, 16] the shape has been shown to influence their biodistribution in the body, pharmacokinetic profile and internalization pathway, and consequently their therapeutic and imaging properties.[17-20] Other examples exist in the literature on the

role of osmotic pressure for biological cells, like the regulation of the plasma membrane tension by large surface area membrane proteins acting as "osmo-valves" to protect the cell against osmotic imbalances,[21] or the production by some fungi spores of osmotic agents (*e.g.* glycerol) to pierce the leaves of plants,[22] which more generally remain turgescent thank to the osmotic pressure of water acting on their cell walls. As polymersomes generally present very selective permeabilities,[23] a difference in permeation rate of species can easily trigger an osmotic imbalance between the inner and the outer media, thus potentially inducing shape modification or even vesicle rupture. It is then of prime importance to precisely elucidate this osmotic pressure induced phenomenon in order to better anticipate and define the behavior of polymersomes in complex biological conditions.

The osmotic pressure gradient across a membrane is related to the difference between the osmolarity of the internal medium and the external medium: $\Delta\Pi = RT(c_{int} - c_{ext}) = RT\Delta c$. In the pioneering work of E. Boroske and W. Helfrich, the osmotic shrinkage of giant unilamellar vesicles (GUV) under hypertonic conditions (negative osmotic pressure difference $\Delta\Pi$) observed as a function of time by optical microscopy appeared as an efficient method to measure the permeability constant of water through the membranes.[24] Both lipid and polymer vesicles have also been shown to undergo swelling in hypotonic conditions (positive osmotic pressure difference $\Delta\Pi$), leading in some cases to a burst process,[25] with a possible reseal of the membrane after leakage.[26, 27] Vesicle behaviors under hypertonic stress appear to be more complex. According to experimental and theoretical studies[28, 29] giant unilamellar liposomes, when exposed to hypertonic conditions, evolve from spheres into a variety of non-spherical morphologies, such as prolate or oblate ellipsoids, stomatocytes and even into non-axisymmetric starfish shapes.[30, 31] The formation of "raspberry vesicles" has also been reported for DOPC

(1,2-dioleoyl-sn-glycero-3-phosphocholine),[32] DOPG (dioleoylphosphatidylglycerol)[33] and EPC (egg phosphatidylcholine)[34] GUVs in such conditions due to the excess surface membrane area appearing while volume shrinking and the outward flow-rate of water. All these morphological changes are enabled by the fluidity of the phospholipid bilayer membranes above their main chain transition temperature. An interesting response to hypertonic stresses has been reported for micro-sized catanionic vesicles of icosahedral symmetry by Carrière et al.[35] They observed that when incubated in a hypertonic solution above a hypertonicity threshold (below 1 mOsm) the icosahedral vesicles progressively collapsed until complete buckling. During the last stages of buckling, the encapsulated material was released due to the rupture of the bilayer membrane. SANS experiments and theoretical calculations indicate that this rupture is predominantly governed by curvature and happens when the radius of curvature is comparable to the membrane thickness.

Polymersomes are believed to undergo similar shape transformations than liposomes if the polymer chains in the membrane possess enough mobility in the experimental conditions.[1, 36, 37] However, even with a membrane formed with a hydrophobic block of low glass transition temperature T_g, several behaviors were reported depending on the polymer nature and architecture. The formation of raspberry vesicles was observed for PDMS-*g*-PEO (poly(dimethylsiloxane)-*g*-poly(ethylene oxide)) and PBut-*b*-PEO (polybutadiene-*b*-poly(ethylene oxide)) giant vesicles but non-axisymmetric shape deformations, faceting, or bursting were also evidenced.[26] Lorenceau *et al.* reported a collapsed structure for PBA-*b*-PAA (poly(n-butyl acrylate)-*b*-poly(acrylic acid)) giant vesicles in similar hypertonic conditions.[38] Whereas the thinnest possible membrane of a liposome is always a bilayer made of two lipid leaflets, polymersomes self-assemble

from amphiphilic copolymers into either a bilayer (for diblock or graft copolymers) or a monolayer (for triblocks or even random copolymers). We will see in the following that the membrane structure can strongly affect the vesicle transformations under osmotic shocks.

The vesicle size (related to the radius of curvature of membrane) is actually another additional important factor. Concerning smaller liposomes, instead of the formation of raspberry-like vesicles observed for GUVs, a shape transition from spherical to oblate vesicles in hypertonic conditions has been reported for different phospholipids (DOPC, EPC).[39,40] Studies on DODAB (dioctadecyldimethylammonium bromide) small unilamellar (SUV) liposomes [41] and DODAC (dioctadecyldimethylammonium chloride) SUVs [42] have also shown that the neutral or charged character of the osmotic agent used has an influence on the final morphology. On the one hand, when exposed to a hypertonic media containing $CaCl_2$, these unilamellar vesicles deflated into a stomatocyte shape – *i.e.* concave vesicles shaped like a stomach. As the electrostatic double layer thickness of the membrane was strongly decreased by the high ionic strength of the divalent salt, the repulsion between the cationic charges of the bilayers was screened, and the edges of the stomatocyte progressively approached each other until they fused into a non-reversible bi-lamellar twinned vesicle. On the other hand, a sucrose hypertonic medium only led to "lens-like" deflated structures, as the prerequisites to allow the approach and fusion of the edges were not fulfilled. B. Pitard *et al.* who studied DNA encapsulation in liposomes (lipoplex) did a control experiment by submitting pure liposomes to a hyperosmotic concentration gradient of NaCl (c_{ext}-c_{int} = 150 mM),[43] that led to the formation of bi-lamellar vesicles out of unilamellar ones, some of them being elongated (Figure 4B and 4C of this reference).

Concerning nanosize polymersomes, only a few reports are available in the literature.

Kim *et al.* studied the shape transformation of PS-*b*-PEO (polystyrene-*b*-poly(ethylene oxide)) polymersomes.[44] They evidenced that a partial deflation of these vesicles changes their shape from spheres to stomatocytes, as observed for DODAB liposomes. Surprisingly, no twinned vesicles but collapsed vesicles (the so-called "kippah" morphologies)[45] were observed when the volume was further decreased.[46]

It is thus becoming obvious that osmotic-induced stresses are able to shape the polymersomes in different ways. Understanding the parameters that control these morphological changes in such conditions is then necessary to precisely design polymersomes as drug delivery devices or cell-mimicking assemblies of precise shapes and anticipate their behavior in complex biological media. In this context, we were interested in describing how the copolymer architecture – grafted *versus* triblock – and thus the membrane structure – bilayer *versus* monolayer – influence these deformations. In particular, we will evidence in the following that fluid polymersomes made of a graft copolymer transform into original bi-lamellar "double" polymersomes after intermediate stomatocyte formation and ultimate membrane fusion. On the contrary for vesicles made of a triblock copolymer, no such double polymersomes were found, presumably due to the polymer architecture that disfavors the membrane fusion. Interestingly, these results are obtained by two independent complementary experimental approaches in order to avoid multiple artifacts. One is cryo-transmission electron microscopy (cryo-TEM) for direct imaging of the geometrical shape of the objects, and the other is small angle neutron scattering (SANS) to measure better averaged nanoscopic dimensions of the objects through an appropriate model. This work is therefore original by giving a very precise and quantitative insight on the relationship between vesicular shape transformation and macromolecular design.

Results and Discussion.

Polymersomes under hyper and hypotonic conditions observed by DLS. Changes in apparent hydrodynamic radii of PDMS-*g*-PEO and PEO-*b*-PDMS-*b*-PEO vesicles upon osmotic shocks have been measured by DLS on samples at 1 mg/mL. The vesicles were prepared at 10 mg/mL – based on procedures described in the experimental part – and their initial hydrodynamic size (R_0) was measured on samples diluted by an isotonic aqueous solution (à virer car le 1M sème la confusion: c'est expliqué dans les procedures). The second hydrodynamic radius measurement (R_H), done one hour after applying the shock by adjusting the external glucose concentration, allowed determining any changes in size induced by the osmotic pressure. Vesicles were always submitted to a single osmotic shock with no consecutive changes of the external medium.

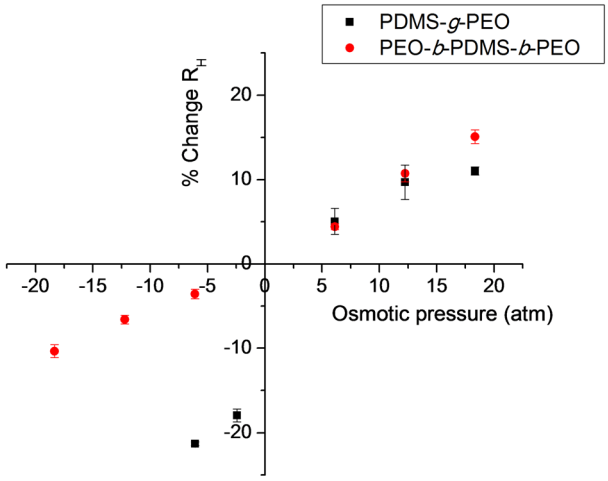

Figure 1. Evolution of vesicles hydrodynamic radius R_H under osmotic conditions measured by DLS (measurements are in triplicate). The percentage of change of R_H corresponds to the relative change $(R_H\text{-}R_0)/R_0$, R_0 being the initial radius. All samples were prepared at 1 mg/mL. Osmotic shocks and the beginning of measurements were separated by a 1-hour delay.

Table 1. Hydrodynamic radius (R_H) and polydispersity index under several osmotic conditions measured by DLS.

Shock	Hypertonic				Isotonic		Hypotonic	
Δc (mM)	-750	-500	-250	-100	0	250	500	750
$\Delta \Pi$ (atm)	-18.3	-12.2	-6.1	-2.4	0	6.1	12.2	18.3
Sample	Hydrodynamic radius R_H (nm) and polydispersity index							
PDMS-*g*-PEO	-	-	42.8 ± 0.1 (0.06)	44.6 ± 0.4 (0.09)	54.4 ± 0.5 (0.05)	-	-	-
	-	-	-	-	44.6 ± 0.5 (0.04)	46.8 ± 0.7 (0.03)	48.9 ± 0.9 (0.03)	49.5 ± 0.2 (0.03)
PEO-*b*-PDMS-*b*-PEO	44.2 ± 0.4 (0.06)	46.1 ± 0.3 (0.06)	47.6 ± 0.3 (0.06)	-	49.3 ± 0.3 (0.05)	-	-	-
	-	-	-	-	50.3 ± 0.6 (0.14)	52.5 ± 0.2 (0.11)	55.7 ± 0.5 (0.14)	57.9 ± 0.4 (0.12)

The evolution of the vesicles hydrodynamic radii upon positive or negative osmotic shocks shown in Figure 1 confirmed that hypertonic stresses resulted into a shrinking of the vesicles and hypotonic stresses into a swelling. PDMS-*g*-PEO vesicles were the most responsive in hypertonic conditions, changes in diameter reached -21.3% as compare to the ~ -10% for the triblock copolymer vesicles even though the applied osmotic pressure was higher. The sudden drop of radius observed for the former vesicles, even at a hypertonic pressure of 2 atm, could be attributed to the morphological transformation from unilamellar to bi-lamellar vesicles. The osmolarity between the two media was ~~re-equilibrated~~ modified (actually it is never re-equilibrated !) by water transfer through the membrane.[24, 26] In hypotonic conditions, the solute concentration inside the vesicle was higher than in the external medium, so that water came into the vesicle, resulting into a swelling. On the contrary, in hypertonic conditions water was pushed out of the vesicles, resulting into a decrease of their diameter. It necessarily implies an excess of surface membrane area, but the membrane reorganization cannot be appreciated by light scattering results only

since a true interpretation of a hydrodynamic radius is function of the object shape. In order to get more insight on the structural changes at nanoscale induced by an osmotic stress, vesicles under such conditions were further studied by cryo-TEM and SANS. Under hypotonic shocks, neither membrane thickening nor significant changes of vesicle radii for PDMS-*g*-PEO vesicular solutions were observed by SANS (curves shown in Electronic Supporting Information, Fig. S1b). In the following, we then focus on the structural changes upon hypertonic conditions. For PDMS-g-PEO vesicles, that were the more responsive to changes, hypertonic glucose concentration gradients chosen were 100 mM and 250 mM (equivalent to the external solution osmolarity as vesicles were originally water-filled). For the triblock copolymer, 250 mM and 750 mM hypertonic conditions were selected. The equivalent osmotic pressures are higher than conditions usually encountered in natural media (of order ??) but were chosen to better evidence the influence of membrane parameters on the shape evolution.

PDMS-g-PEO structural changes in hypertonic conditions. Figure 2-A shows typical cryo-TEM image of PDMS-*g*-PEO vesicles in their native state (isotonic conditions, *i.e.* pure water). Vesicles appeared to be polydisperse in size and shape, a non-negligible part of them being found anisotropic as evidenced by the aspect ratio distribution. This is likely an effect of the extrusion step as already reported for lipidic systems,[47] where vesicles larger than the pore size are deformed while passing through the extrusion filter and eventually break up. Once on the other side of the filter, they reseal but can retain an anisotropic shape due to the excess of surface membrane area. A statistical study (over a number of structures n = 148) revealed that 96% of the objects were unilamellar vesicles. Indeed, the difference between simple (unilamellar) and double (bi-lamellar) membrane is clear on cryo-TEM images, since silicon atoms of

PDMS provide an electron scattering density sufficiently different from the carbon and oxygen atoms of PEO. The experimental uncertainty, determined by measuring several times the same membrane thickness, was below one nanometer. An average membrane thickness of 5.4 ± 0.6 nm (number of measurements *n* = 50) was measured, in good agreement with the value of about 5 nm reported in literature for PDMS-*g*-PEO unilamellar vesicles.[48]

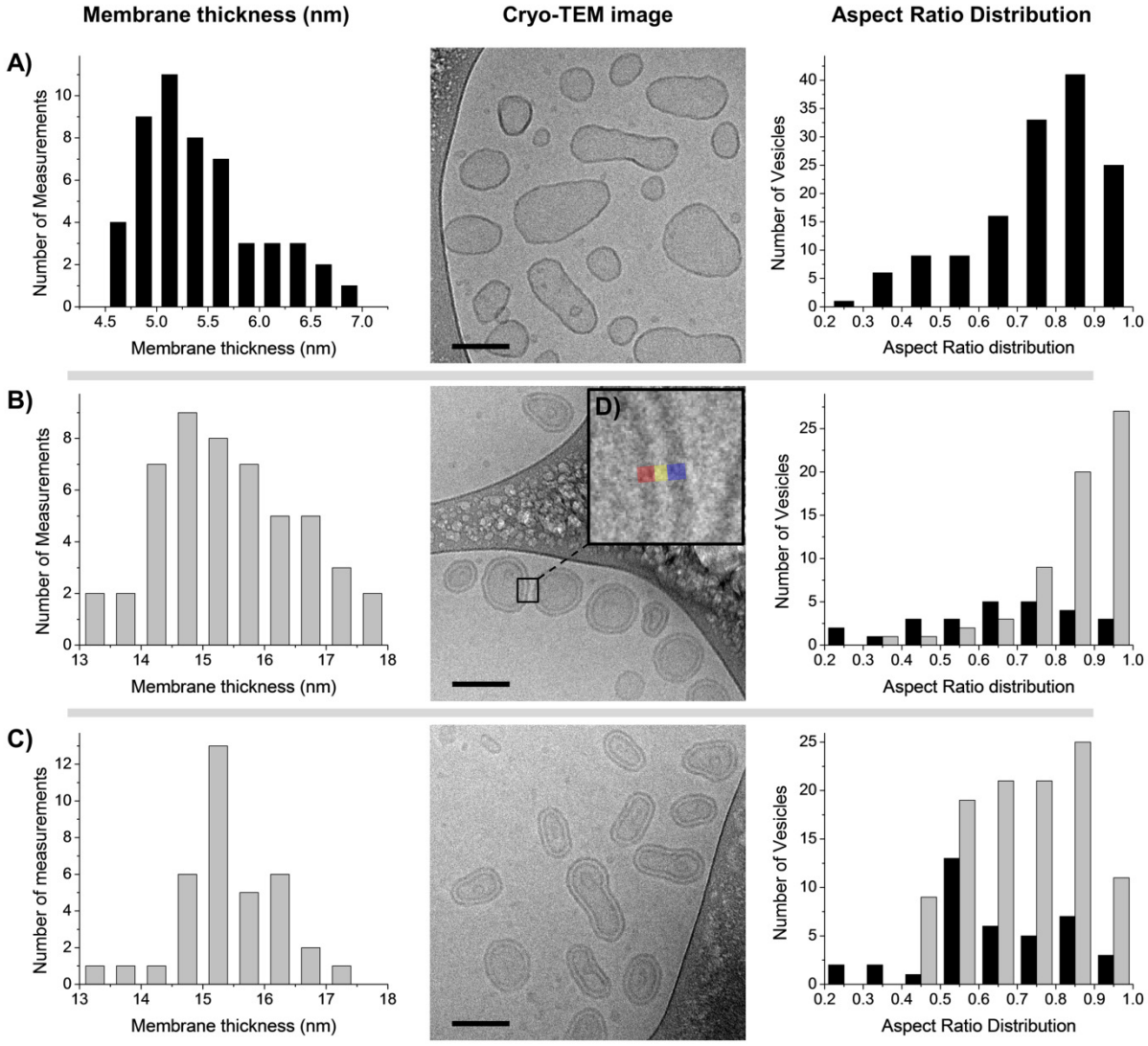

Figure 2. Membrane thickness measurements, cryo-TEM images (scale bars represent 100 nm) and aspect ratio distribution of PDMS-*g*-PEO vesicles under different osmotic conditions. Water-filled vesicles were originally (A) in pure water, and then the external glucose concentration was adjusted to (B) 100 mM or (C) 250 mM to apply a hypertonic

shock. On all diagrams, black columns represent unilamellar vesicles and grey columns represent bi-lamellar nested vesicles. For samples in hypertonic conditions (B and C), the membrane thickness was measured on nested vesicles and represents the total width including the two polymer layers and the water gap (δ_{tot}). (D) Insert: zoom on the vesicle membrane. The red area corresponds to the internal shell thickness δ_i, the yellow one to the water gap D_w and the blue one to the external shell thickness δ_e. Using the ImageJ software, the projection of vesicles in the observation plane were approximated by ellipsoids of semi-major axis a, semi-minor axis b, thus aspect ratio $K=b/a$.

Table 2. Cryo-TEM and SANS structure parameters as measured for PDMS-*g*-PEO water-filled vesicles under various osmotic conditions.

		Cryo-TEM			SANS						
Δc	Membrane	δ_{tot} (nm)	$\delta_{i/e}$ (nm)	D_w (nm)	Model	R_c (nm)	σ_{Rc}	δ (nm)	σ_δ	D_w (nm)	σ_{Dw}
0 mM	Unilamellar	5.4 ± 0.6	-	-	Vesicle	33	0.38	5.75	0.12	-	-
100 mM	Bi-lamellar	15.5 ± 1.1	5.6 / 6.1 ± 0.6	3.6 ± 0.9	Mix	16.6	0.33	6.2	0.1	3.9	0.3
250 mM	Bi-lamellar	15.4 ± 1.1	5.9 / 6.0 ± 0.7	3.5 ± 0.7	Mix	16	0.36	5.7	0.1	4.5	0.3

In table 2, the glucose concentration gradients used for the hypertonic shocks are indicated in absolute values and correspond to the osmolarity of the external solution as vesicles were water-filled. For cryo-TEM measurements, δ_i and δ_e are the internal and external layer thicknesses, separated by a water gap D_w; and $\delta_{tot} = \delta_i + D_w + \delta_e$ is the total bi-lamellar membrane thickness. For SANS, R_c is the core radius of the vesicles and δ is the thickness of both polymer layer of the membrane (δ_i and δ_e are assumed identical), σ_{Rc}, σ_δ, and σ_{Dw} being the widths of respectively the Log-normal distributions of R_c, δ, and D_w.

Cryo-TEM images of the system after having adjusted the external glucose concentration to 100 mM (Figure 2-B) show a large majority of nested polymersomes, *i.e.* vesicles with a bi-lamellar membrane formed by two polymer layers fully separated by a water gap. A statistical study (n = 93) revealed that 72% of structures were nested vesicles and their aspect ratio K distribution shows that they are more spherical (K closer to 1) that unilamellar vesicles before the shock. As the two layers can easily be distinguished on cryo-TEM images, several membrane thickness

measurements were carried out (figure 2-D). Internal and external thicknesses of shells, respectively δ_i = 5.6 ± 0.6 nm and δ_e = 6.1 ± 0.6 nm (n = 50), were found similar to the membrane thickness of unilamellar vesicles determined before applying a hypertonic shock (Table 2). The distance between these two shells was found rather constant at a value D_w = 3.6 ± 0.9 nm. Then, the total bi-lamellar membrane thickness was found to be $\delta_{tot} = \delta_i + D_w + \delta_e$ = 15.5 ± 1.1 nm. Vesicles that stayed unilamellar, about 28%, were stretched out and appear to be smaller than nested vesicles on cryo-TEM images, as confirmed by the initial radius calculation presented later on.

The strongest applied hypertonic shock (Figure 2-C), with a glucose concentration gradient of 250 mM, led to a similar vesicles population distribution since nested vesicles represented 74% of the structures observed (n = 151) and the remaining unilamellar vesicles 26%. Membrane thicknesses measurements (n = 38) also gave results similar to the hypertonic shock with a 100 mM glucose solution as external medium (Table 2). The main difference, confirmed by the aspect ratio K distribution, is that these nested vesicles were now stretched out and not spherical anymore.

Observation of nested polymersome structures in such conditions is in agreement with DLS measurements provided that the change in shape is taken into account to recalculate the external diameter and compare it to the initial hydrodynamic radius. Using measured membrane parameters and from pure geometrical considerations, one can indeed calculate the decrease in external radius of unilamellar vesicles that would undergo these morphological changes, the parameter set constant being the surface membrane area. For an initial radius R_0 of 54 nm, a polymer layer thickness of 5.5 nm and 3.5 nm between the shells after transformation, it would result in a 21.5% decrease of the external radius. This value is in good agreement with the decrease in

hydrodynamic radius measured by DLS – 17.9% and 21.3% for the 100 mM and 250 mM hypertonic shocks respectively.

These bi-lamellar vesicles were further investigated using SANS, in order to obtain a more detailed analysis of the membrane characteristics at nanoscale averaged on many objects and to rule out any cryo-TEM preparation artifact or statistical bias. Figure 3-A shows the scattered intensity per unit volume for PDMS-*g*-PEO vesicles in their preparation media, *i.e.* pure D_2O at room temperature. The vesicular morphology of this sample is characterized by the q^{-2} decrease of the SANS intensity in the intermediate q values regime. In such conditions, the experimental data were fitted with a polydisperse hollow sphere form factor using the SasView program (http://www.sasview.org/) using a proper weighting of the hollow sphere form factor (1) by the volumes (2) with Log-normal distribution laws of both the core radius R_c and of the membrane thickness δ(3). The form factor (tending towards 1 when q→0) is given by :[49]

$$P(q,R_c,R_e)=\frac{9}{\left(V_{R_e}-V_{R_c}\right)^2}\left[V_{R_e}\frac{\sin\left(qR_e\right)-qR_e\cos\left(qR_e\right)}{\left(qR_e\right)^3}-V_{R_c}\frac{\sin\left(qR_c\right)-qR_c\cos\left(qR_c\right)}{\left(qR_c\right)^3}\right]^2 \quad (1)$$

The scattered intensity in absolute units (cm^{-1}) is proportional to polymer volume fraction and neutron contrast with the solvent and calculated by integrating the geometrical polydispersity:

$$I\left(q\right)=\Phi\left(\Delta\rho_n\right)^2\frac{\iint_{R_c,\delta}\left(V_{R_e=R_c+\delta}-V_{R_c}\right)^2P(q,R_c,R_e=R_c+\delta)\,F(R_c,\sigma_{R_c})dR_c\;F(\delta,\sigma_\delta)d\delta}{\iint_{R_c,\delta}\left(V_{R_e=R_c+\delta}-V_{R_c}\right)F(R_c,\sigma_{R_c})dR_c\;F(\delta,\sigma_\delta)d\delta} \quad (2)$$

with Log-normal distributions laws both for the core radius $F(R_c, \sigma_{Rc})$ and for the shell thickness $F(\delta, \sigma_\delta)$:

$$F(x,x_0,\sigma_x)=\frac{1}{\sqrt{2\pi\sigma_x}x}\exp\left[\left(-\frac{1}{2\sigma_x^{\,2}}\left(\ln\frac{x}{x_0}\right)^2\right)\right] \quad (3)$$

In these formulas, R_c and $R_e = R_c + \delta$ respectively correspond to the core radius and the external radius of the shell, and $V_{Rc}(V_{Re})$ is the volume of the sphere of radius $R_c(R_e)$. For $q \to 0$, the intensity $I(q)$ tends towards

$$I(q) \xrightarrow[q\to 0]{} \Phi(\Delta\rho_n)^2 \left\langle \left(V_{R_e=R_c+\delta} - V_{R_c}\right)^2 \right\rangle \Big/ \left\langle V_{R_e=R_c} \right\rangle$$

where the brackets represent statistical averages. All scattering objects are considered to be PDMS shells, with a scattering length density $SLD_{PDMS} = 6.37\times10^{-8}$ Å^{-2}, into a D_2O media of $SLD_{D2O} = 6.35\times10^{-6}$ Å^{-2}. The polydispersity in shape and size, revealed by cryo-TEM analysis, cannot be distinguished with this technique so resulted in a weak influence of the vesicle radius value on the quality of the fits. On the contrary, the fit results were very sensitive to the membrane parameters (its median thickness δ, and standard width of the Log-normal distribution, σ_δ). The best results, summarized in Table 2, are obtained for a core radius $R_c = 33$ nm ($\sigma_{Rc} = 0.38$) and a membrane thickness $\delta = R_e - R_c = 5.75$ nm ($\sigma_\delta = 0.12$), which agrees well with cryo-TEM observations, and also confirms that vesicles were mostly unilamellar after the extrusion process.

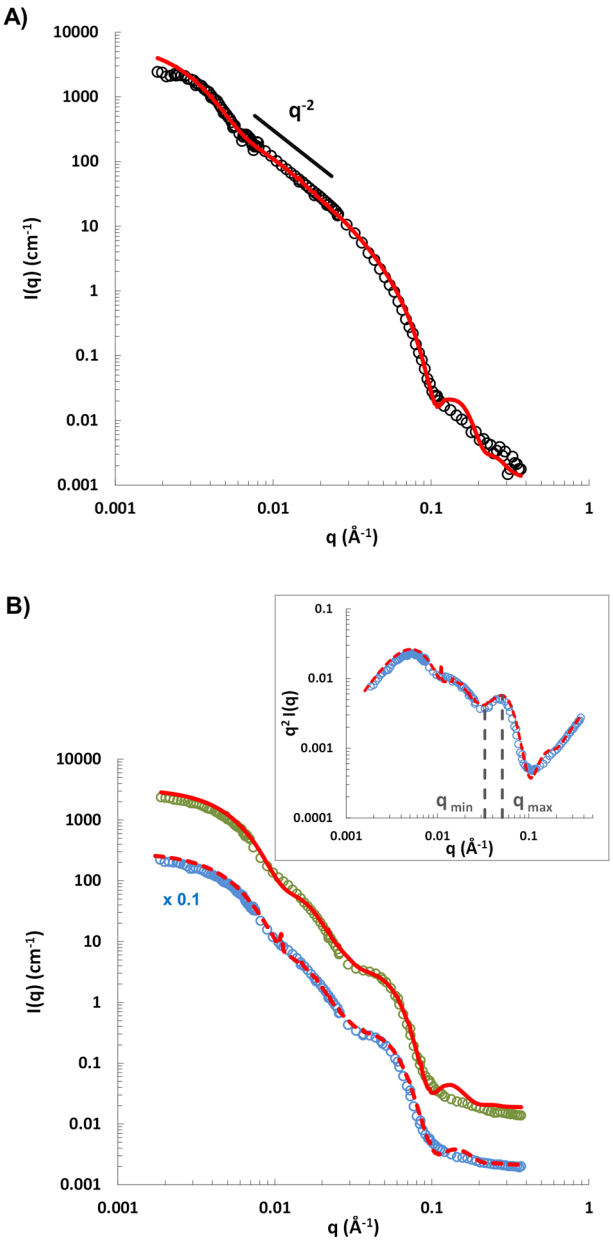

Figure 3. Small angle neutron scattering of PDMS-*g*-PEO vesicles initially prepared at 10 mg/mL in D_2O. A) Experimental data in isotonic conditions, the full line is a fitting curve by a polydisperse hollow spheres

model (R_c = 33 nm, δ = 5.75 nm). B) Scattered intensity for the same samples after being submitted to a hypertonic stress with a glucose concentration gradient of 100 mM (green dots) or 250 mM (blue dots, data have been vertically shifted (×0.1) for clarity). The full line and dashed line are fitting curves by a mixed model of polydisperse multi-shells and hollow spheres for the 100 mM and the 250 mM osmotic shocks respectively. The inset is the $I(q)\times q^2$ *vs*. q representation for the experimental data and the fitting curve of the 250 mM hypertonic shock.

Experiments carried out on the same sample after applying a hypertonic stress revealed a strong undulation of the scattered intensity in the intermediate q regime (Figure 3-B). The local maximum of the curve (on a $I(q)\times q^2$ scale) at a wave-vector $q_{max}\sim5\times10^{-2}$ Å is very similar for both shocks, and indicates that the two samples have a similar characteristic length of the membranes $\pi/q_{max}\sim60$ Å very close to the membrane thickness measured by cryo-TEM or SANS. Even if a decrease in vesicle radius could be deduced from the change in position of the oscillations at low q, values cannot be used to quantify the shrinkage of the vesicles because of the polydispersity in sizes and shapes, as observed by cryo-TEM. Experimental data can be fitted with a Multi Shell Model provided in SasView software. It consists in two spherical shells of same center, identical in layer thickness ($\delta_i=\delta_e=\delta$) and scattering length density as cryo-TEM experiments evidenced, separated by a layer of solvent (D_w, Figure S2). Once again, results showed little dependence on the whole vesicle radius value, but were very sensitive to membrane parameters, justifying the choice of SANS to follow the reorganization of membranes with a high precision. For the sample shocked with an osmolarity of 100 mM, fit results with this model lead to a core radius R_c = 16.6 nm (σ_{Rc} = 0.33) around twice as low as in isotonic conditions. The determined thickness of the two shells, δ = 6.2 nm (σ_δ =

0.1), and the distance between them D_w = 3.9 nm (σ_{Dw} = 0.5) are in excellent agreement with values measured on cryo-TEM images. Despite the high polydispersity of the distance between the two shells (σ_{Dw} = 0.5), the amplitude of the oscillation of the simulated curve in the intermediate q regime was still too high (too low intensity at q_{min}) compare to the experiment. Therefore, we mixed the two models (unilamellar and bi-lamellar) to take into account the presence of remaining unilamellar vesicles in the sample (as observed by cryo-TEM on Figure 2-B) and to achieve a proper fit of the experimental intensity. The best fit, presented in figure 3-B, was indeed obtained by adding simulated curves for unilamellar and nested vesicles using parameters previously determined by SANS and cryo-TEM. All fitting parameters were kept identical for nested vesicles, except σ_{Dw} set at 0.3. Unilamellar vesicles were simulated by a Hollow Sphere Model with the same radius and membrane parameters as nested vesicles (but only one shell), and the proportion of each population was fixed using the repartition measured by cryo-TEM: 72% of nested vesicles and 28% of unilamellar vesicles. Concerning the sample shocked with an osmolarity of 250 mM, the best fit is also a mix of nested (74%) and unilamellar vesicles (26%). Fitting parameters (Table 2) are similar to those of the 100 mM hypertonic shock and confirm that membranes parameters were the same for the two hypertonic conditions.

These SANS experiments confirm that when submitted to a hypertonic stress ranging from 100 mM to at least 250 mM, water-filled PDMS-*g*-PEO unilamellar vesicles change their structure to form nested vesicles with a constant distance between the two polymer layers constituting the membrane. Membrane parameters determined by SANS for nested vesicles are in excellent agreement with the cryo-TEM experiments and confirm the physical meaning and robustness of our fits. Moreover, these results show that statistical

weights and geometrical parameters measured independently using cryo-TEM can be used to fit neutrons scattering experimental data in a very quantitative way.

The force driving the shape transformation during hypertonic shock is the decrease in the volume of the inner compartment of the polymersomes. The Area Difference Elasticity model (ADE) uses the reduced volume as one of the critical parameters to predict vesicle shape transformation upon shrinking and swelling.[29] This reduced volume corresponds for a given membrane surface area (A) to the ratio between the inner volume enclosed by the membrane (V) and the volume of a sphere with the same area: $v=3(4\pi)^{1/2}V/A^{3/2}$. According to predicted shape trajectory in the ADE model, spherical vesicles ($v=1$) evolve to stomatocytes once the reduced volume reduces to a value close to 0.59. Then, while the reduced volume is further decreased, the two parts of the stomatocyte that approach each other come into close contact, and eventually fuse, which reorganizes the shape of the vesicle and leads to the formation of a nested vesicle. During this transformation, a volume of the external solution becomes encapsulated in the new nested vesicle, while the former internal solution constitutes the water gap D_w between the two membranes (Figure 4). No transient stomatocytes could be observed as changes occurred within seconds. However it is believed that vesicles evolved through this shape evolution trajectory, as proposed by Hubert *et al.*[41] for DODAB vesicles. Cryo-TEM observations confirm this pathway, as only closed structures were observed on the micrographs. In addition, defects resulting from the membrane fusion, like internal buddings or scars, can be seen on some nested vesicles (Figures S3 & S4), also in agreement with this mechanism of transformation.

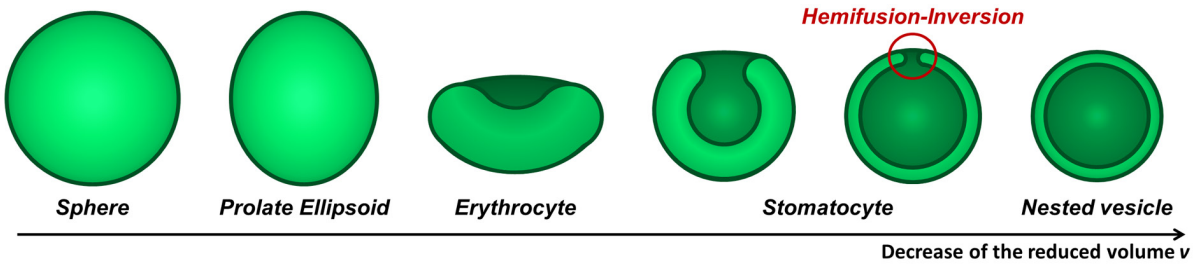

Figure 4. Sketch of the transformation pathway by osmotic deflation of an initially spherical vesicle though the stomatocyte shape, leading finally to the bi-lamellar "nested" vesicle as a function of the reduced volume *v*. The white green and dark green represent respectively the initial internal and external surfaces of the vesicle. All shapes exhibit rotational symmetry along the vertical axis.

The final membrane conformation for water-filled vesicles that undergo this shape transformation is made of two polymer layers separated by an interspace. Indeed, SANS experiments revealed that no changes occurred in the copolymer organization within a single polymer layer: the thickness of each layer in nested structures, about 6 nm, is the same than the membrane of unilamellar vesicles. The remaining inner volume, confined between the two layers for such a nested structure, is found the same for the two applied osmotic shock, meaning that it was as reduced as possible and reached a limit. This minimal separation, that seems to be water-filled according to SANS experiments, is probably governed by steric hindrance between the hydrated PEO chains covering each layer. Theoretically, as long as the bending energy does not compensate the osmotic pressure, this conformation should be reached whatever the hypertonic pressure. Indeed, the osmotic imbalance for water-filled vesicles cannot disappear while the original vesicle is not empty. If the vesicle encapsulates a solute, the morphology should follow the shape evolution trajectory predicted by the ADE model until reaching the reduced volume that allow the equilibrium of the osmolarity between the internal and external medium.

Then, it is possible to precisely tune the shape of such nano-vesicle once injected in a physiological media (~300 mOsm) by carefully choosing the initial internal solute concentration.

However, some limitations of theoretical models are reached because of the small size of the polymersomes prepared through an extrusion process. Indeed, the membrane thickness becomes no more negligible with respect to the vesicle radius and thus the membrane cannot be seen as a 2D surface embedded in 3D space as hypothesized in the ADE model.[29] Careful examination of cryo-TEM images revealed that unilamellar vesicles that are still present after hypertonic stresses are stretched out and smaller than the nested vesicles. This may be due to a higher bending energy when the membrane thickness becomes of the same order of magnitude than the radius of curvature: such a finite-size effect that would prevent the formation of an invagination for significantly curved vesicles has not been encountered yet, to the authors' knowledge, by the current theoretical predictions including those that consider confinement effects.[50, 51] One can thus try to estimate if a minimal radius before applying a hypertonic shock is necessary for the formation of nested vesicle. The initial radius R_0 of each vesicles can be estimated for nested vesicles and stretched out unilamellar ones from their surface membrane area. It corresponds to the radius of a spherical and unilamellar vesicle with the same surface area. As all structures are not spherical, they appear as ellipses on cryo-TEM images, the surface membrane area can only be calculated with an assumption on the 3D vesicle shape. As models on fluid membranes predicts that ellipsoids are prolate for a small excess of membrane area compare to the inner compartment,[29] we assumed that the non-spherical unilamellar and nested vesicles are prolate ellipsoids. Initial radii R_0 can be then estimated with the following equation (Figure S5):

$$R_0 = \left[\sum_i \left(\frac{b_i^2}{2} + \frac{a_i b_i}{2e_i} Arc\sin(e_i) \right) \right]^{\frac{1}{2}}$$

and $$e_i = \frac{\sqrt{a_i^2 - b_i^2}}{a_i}$$

with a_0 = semi-major axis and b_0 = semi-minor axis of the fitting ellipse for all the vesicles, and $a_1 = a_0 - (\delta + D_w)$ and $b_1 = b_0 - (\delta + D_w)$ for nested vesicles only. For calculations, the membrane thickness is δ = 5.8 nm and the water gap between the shells D_w = 3.5 nm (average values from all cryo-TEM measurements in table 2). A minimal initial radius needed to form a nested vesicle $R_{0\ min}$ could be determined for each hypertonic condition from the smallest R_0 value of nested vesicles. Determined values are $R_{0\ min}^{100\ mM}$ = 23.7 nm for the hypertonic shock with a 100 mM solution and $R_{0\ min}^{250\ mM}$ = 22.9 nm for the shock at 250 mM. These values correspond to maximum ratios $(\delta/R)_{max}^{100\ mM}$ = 0.24 and $(\delta/R)_{max}^{250\ mM}$ = 0.25. Interestingly, there is a good agreement between the minimal R_0 calculated values and the radii R_0 measured by cryo-TEM on unilamellar vesicles remaining after hypertonic shock. This is a consequence of the non-negligible membrane thickness compared to radius: above a maximal ratio (δ/R), vesicles do not follow the same shape evolution trajectory. Finally it is interesting to note that nested structures can only be obtained for a certain range of sizes as it has been clearly shown that giant vesicles present raspberry-like[26, 32-34] structures under hypertonic shock and that very small vesicles ($R_0 < R_{0\ min}$) only present ellipsoid shape when they undergo hypertonic shock (figure 5).

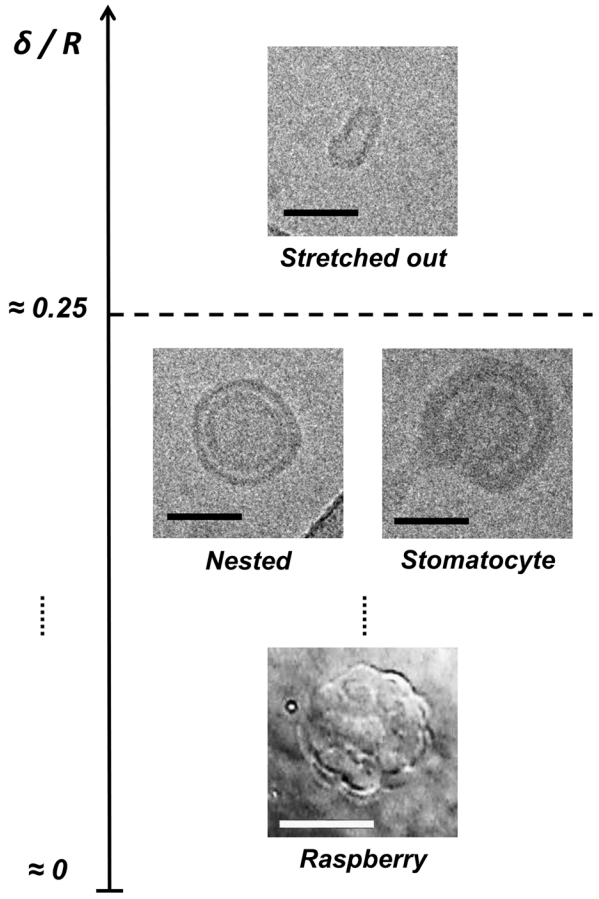

Figure 5. Final morphology expected for water-filled vesicles with a fluid membrane submitted to a hypertonic stress as a function of the membrane thickness / vesicle radius ratio. Illustration is made using the cryo-TEM image of a PEO-*b*-PDMS-*b*-PEO vesicle (middle, right image), cryo-TEM images of PDMS-*g*-PEO vesicles (top and middle, left image) and a DIC microscopy image of a PDMS-*g*-PEO raspberry vesicle (bottom image, adapted from[26]). Black scale bars represent 50 nm and white scale bar 20 µm.

With this evolution pathway depicted on Fig. 4, the external medium becomes the internal phase, and final objects are perfectly isotonic. Thus, the obtained structures should be spherical whatever the initial aspect ratio of the unilamellar vesicle and the applied osmotic shock. This was observed for the 100 mM hypertonic shock. However it is not fully understood why the polymersomes after 250 mM hypertonic shock led to rather stretched out nested vesicles. We propose that at this quite high concentration, glucose may interact with the PEO chains, as already reported,[52] and modifies the spontaneous curvature, slightly changing the shape evolution trajectory effectively followed (the spontaneous curvature c_0 is indeed one of the parameters of the ADE model in addition to the reduce volume *v,* together with the difference of number of amphiphilic molecules between the two bilayer leaflets).[29]

PEO-b-PDMS-b-PEO structural changes in hypertonic conditions.

As observed by DLS on figure 1, water-filled nano-vesicles of PEO-*b*-PDMS-*b*-PEO exhibit only very little changes when submitted to hypertonic stresses, and their slight decrease in hydrodynamic radius of about 10% seems less compatible with the double-layered structure observed for water-filled PDMS-*g*-PEO vesicles. In order to confirm this behavior and understand what parameters govern this moderate response to osmotic stress, cryo-TEM and SANS analyses were also carried out on these polymersomes made of a triblock copolymer.

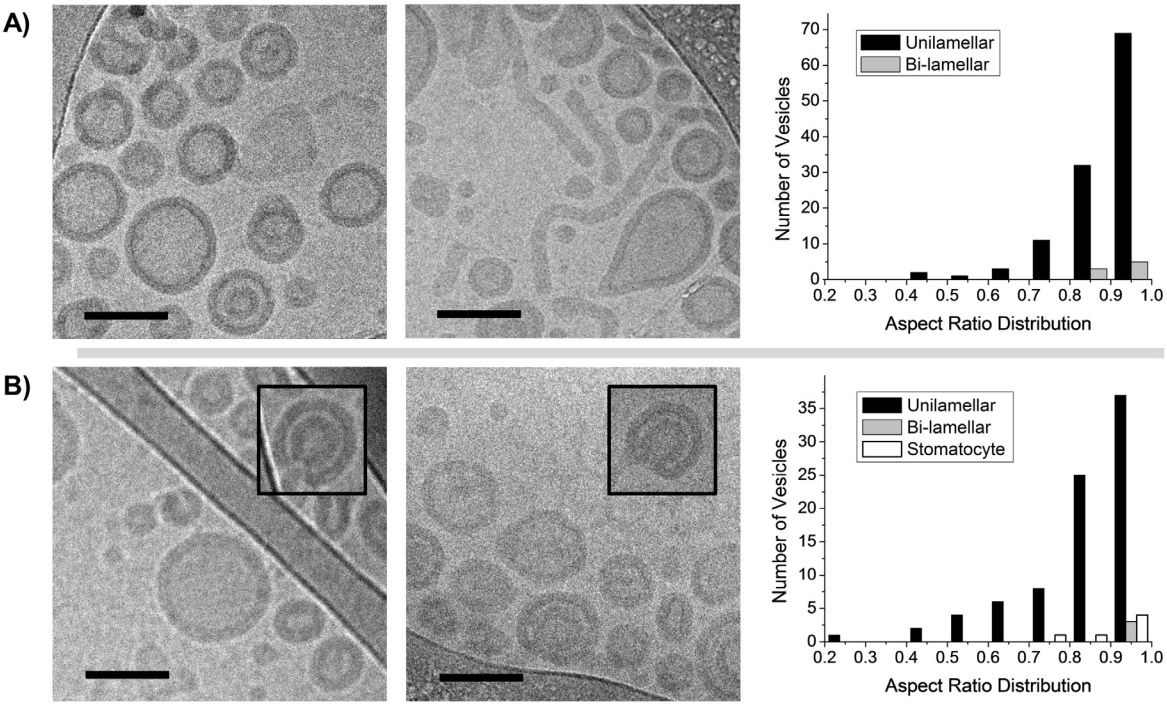

Figure 6. Two different cryo-TEM images and aspect ratio distribution of water-filled PEO-*b*-PDMS-*b*-PEO vesicles in (A) their native state and (B) under 250 mM hypertonic conditions ($\Delta\Pi$ of -6.1 atm). On the aspect ratio diagrams, black columns represent unilamellar vesicles, grey columns represent bi-lamellar vesicles and white columns represent stomatocytes. Inserts in (B) images are other structures observed on the same images, outside the field of view presented here. Scale bars represent 100 nm.

Table 3. Cryo-TEM and SANS structure parameters as measured for PEO-*b*-PDMS-*b*-PEO water-filled vesicles under various osmotic conditions.

Cryo-TEM			SANS					
Δc	Membrane	δ (nm)	Model	R_c (nm)	σ_{Rc}	δ (nm)	σ_{δ}	δ_{KP} (nm)
0 mM	Unilamellar	11.2 ± 1.2	Core Multi Shell	14.9	0.54	11.4	0.12	11
250 mM	Mix	13.6 ± 1.1	Core Multi Shell	10.5	0.54	11.7	0.14	-
750 mM	-	-	Core Multi Shell	10.1	0.55	12.5	0.15	-

In table 3, the glucose concentration gradients used for the hypertonic shocks are indicated in absolute values and correspond to the osmolarity of the external solution as vesicles were water-filled. R_c is the core radius of the vesicles, δ is the membrane thickness and δ_{KP} the membrane thickness determined in the asymptotic Kratky-Porod regime.

Figures 6-A shows typical cryo-TEM images of PEO-*b*-PDMS-*b*-PEO objects in isotonic condition (pure water). It appeared that unilamellar vesicles were not the only population in the system. A statistical study (n = 265) gave the following repartition: 66.8% of unilamellar vesicles, 23.4% of wormlike micelles and 3.8% of closed bi-lamellar vesicles (other structures were clustered vesicles). It is not possible to be sure about the real shape of these bi-lamellar structures resulting from the formation process. If the axis of symmetry of a stomatocyte was indeed oriented in the z-axis direction, it looked like nested vesicles. However, only closed structures were observed, so that it is reasonable to assume that the 3.8% population corresponds to nested bilamellar vesicles. Except worms, vesicles appeared to be mostly spherical and measurements gave an average membrane thickness of about δ = 11.2 ± 1.2 nm (n = 50) (Table 3), in good agreement with a reported value of 10 nm for a similar triblock copolymer with PDMS as central hydrophobic block.[53]

Images of the system after being submitted to a 250mM hypertonic shock (Figure 6-B, $\Delta\Pi$ of -6.1 atm) show quite a number of differences. Stomatocytes were now observed and wormlike micelles almost disappeared. Looking more precisely to the proportion of each structure (n = 137), unilamellar vesicles represent now

81.6% of the total structures, double-layered structures – *i.e.* closed bi-lamellar vesicles and stomatocytes – 11.3% and wormlike micelles only 5%. Membrane thickness of unilamellar vesicles was about δ = 13.6 ± 1.1 nm (n = 50).

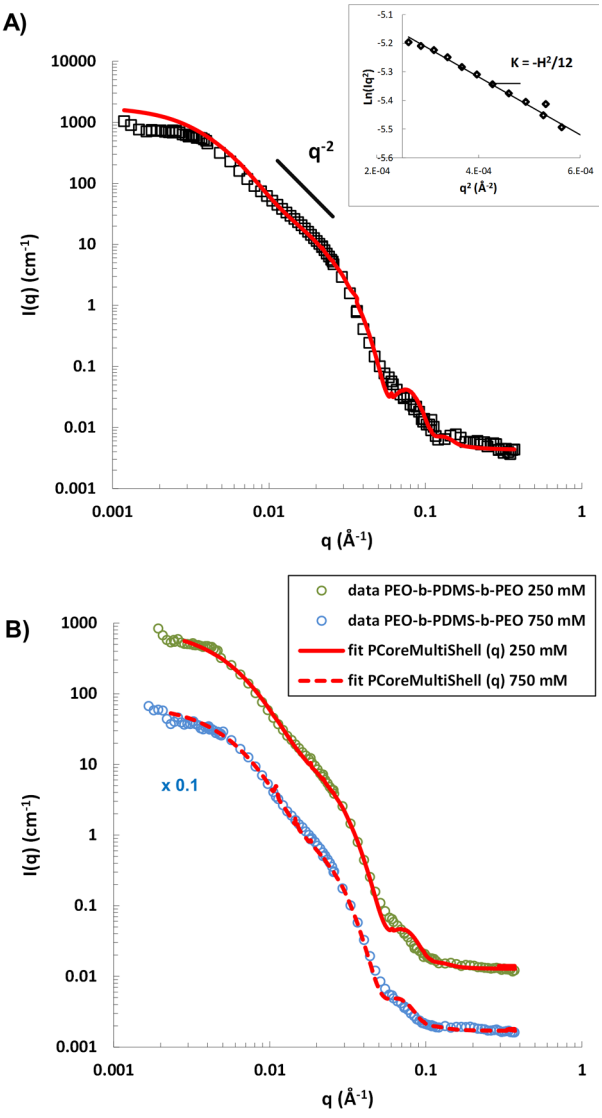

Figure 7. Small angle neutron scattering of PEO-*b*-PDMS-*b*-PEO vesicles initially prepared at 10 mg/mL in D_2O. A) Experimental data in isotonic conditions, the full line is a fitting curve by a core multi-shell model (R_c = 14.9 nm, σ_{Rc} = 0.54, δ = 11.4 nm, σ_δ = 0.12). The inset is the Kratky-Porod plot yielding an estimate of the membrane thickness δ_{KP}. B) Scattered intensity for the same sample after being submitted to a 250 mM or 750 mM hypertonic stress (respectively green and blue dots). The full line and dashed line are fitting curves by a polydisperse core multi-shell model, respectively for the 250 mM (R_c = 10.5 nm, σ_{Rc} = 0.54, δ = 11.7 nm, σ_δ = 0.14) and the 750 mM (R_c = 10.1 nm, σ_{Rc} = 0.55, δ = 12.5 nm, σ_δ = 0.15) hypertonic shocks, corresponding to a $\Delta\Pi$ of -6.1 atm and -18.3 atm respectively.

Figure 7-A shows the SANS scattered intensity for objects in isotonic conditions at room temperature. At intermediate q values, the asymptotic decrease of the scattered intensity varying as q^{-2} evidences the presence of vesicular structures in the sample, but at high q values, the oscillation corresponding to the membrane thickness is less distinct than on Fig. 3 due to a large

polydispersity in sizes and morphologies. From the slope of the representation $\mathrm{Ln}(I(q)\times q^2)$ *vs.* q^2 in the asymptotic Kratky-Porod regime (Figure 7-A Inset), the membrane thickness was estimated to be δ_{KP} = 11 nm, very close to values measured by cryo-TEM (11.2 ± 1.2 nm). Assuming that the major part of the scattered intensity is due to single–wall vesicles composed by the succession of the three blocks of this copolymer, a Core Multi Shell model was used to fit the experimental data (Figure S5). Best fitting parameters indicate a core radius R_c = 14.9 nm (σ_R = 0.54) and a total membrane thickness δ = 11.4 nm (σ_δ = 0.12), again in good agreement with Kratky-Porod approximation and cryo-TEM results (Table 3). Detailed results including neutron scattering length densities (SLD) are reported in Supporting Information Table 1. These fit results evidenced that the vesicles prepared in D_2O had a smaller size than the hydrodynamic radius measured by light scattering experiments, the DLS hydrodynamic size being shifted to higher values by polydispersity, very large as seen from the value of σ_{Rc} = 0.54 in SANS fit.

Measurement on the same sample after applying hypertonic stresses confirmed that no major changes in the objects scattering occurred upon the shock since experimental curves looked very similar (Figure 7-B). The same modeling function with the same conditions of fit parameters was used to fit the experimental data. Core radii parameters did not significantly change the fit quality and were found at small values but with a high polydispersity (Table 3). Determined shell thicknesses are slightly thicker than in isotonic conditions, δ = 11.7 and δ = 12.5 nm for 250 mM ($\Delta\Pi$ = -6.1 atm) and 750 mM ($\Delta\Pi$ = -18.3 atm) hypertonic shocks, respectively. As observed in cryo-TEM, there seems to be a small membrane thickening upon hypertonic shocks.

Notable differences in the evolution of the morphologies under hypertonic stress were found compared PDMS-*g*-PEO vesicles. After applying the hypertonic stress, if the number of structures with a bi-lamellar

membrane was more than twice the initial one, 11.3% of the total structures, more than half of them were clearly identified as stomatocytes (6.4% of the total structures). As there were already nested bilamellar vesicles due to the formation process, this increase in double-layered structures proportion can be mostly attributed to the appearance of stomatocytes and not to newly formed nested vesicles. Moreover, the aspect ratio distribution of unilamellar vesicles was wider than before the shock (Figure 6-B), suggesting that these objects were too small (see below) to form invaginations and thus were just stretched out to reduce their internal volume at a constant surface area.

The lack of sensitivity of this triblock system to hypertonic conditions can be explained by the limitation previously identified: the membrane thickness is not negligible with respect to the vesicle radius. For this system, the minimal initial radius needed to form nested vesicles is $R_{0\ min}^{250\ mM}$ = 39.2 nm, calculated with δ = 11 nm and D_w = 5.5 nm measured for the five smallest nested vesicles after the 250 mM hypertonic shock. It is not surprising to determine a higher $R_{0\ min}^{250\ mM}$ value for the triblock copolymer than for the grafted one, since the energy of a closed membrane is proportional to the bending modulus ($E_b = 8\pi K_b$),[54] the latter being proportional to the square of the membrane thickness.[1] Interestingly, this minimal initial radius $R_{0\ min}^{250\ mM}$ is equivalent to a maximal ratio $(\delta/R)_{max}^{250\ mM}$ = 0.28, close to values determined for PDMS-*g*-PEO vesicles, most likely giving rise to a general thumb rule (not dependent upon the exact polymer architecture) that the radius of curvature needs to be ~4 times larger the membrane thickness to authorize the invagination formation.

Comparing the R_0 values determined for all vesicles remaining unilamellar after the shock with the $R_{0\ min}^{250\ mM}$ value of this system confirms that 85% of them were too small to form nested vesicles and thus were just stretched out. Therefore, the smaller

shrinkage observed by DLS as compared to PDMS-*g*-PEO vesicles (Figure 1) was due to the lack of changes in morphology of these vesicles under hypertonic conditions. This is also the reason why SANS curves on shocked samples for the triblock copolymer vesicles (Fig. 7B) showed almost no change compared to the scattered intensity in isotonic conditions (Fig. 7A).

Surprisingly, the small amount of vesicles which undergo invagination under hypertonic conditions (6.4% of population) never reached a closed bi-lamellar structure and kept their stomatocyte shape, even though the R_0 determined for most of them was higher than $R_{0\ \mathrm{min}}^{250\ \mathrm{mM}}$. A probable explanation of the phenomenon lies in the triblock architecture of the PEO-*b*-PDMS-*b*-PEO copolymer, which leads to the formation of a well-defined copolymer monolayer and not to a bilayer classically formed by diblock copolymers. This monolayer nanostructure disfavors the stomatocyte closure because all the PEO-*b*-PDMS-*b*-PEO chains involved in the hemi-fusion step would have to go through a very unfavorable hairpin conformation to avoid contact between the PDMS hydrophobic core and water, thus increasing the energetic cost of the membrane fusion (Figure 8).

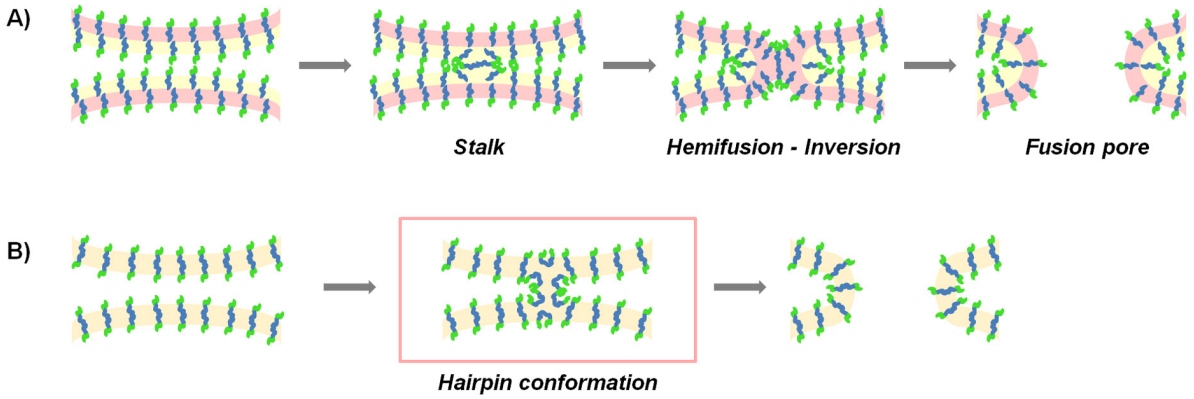

Figure 8. Sketch of the membrane fusion step for membranes formed by A) diblock copolymers and B) triblock copolymers. It is believed that the hemifusion-inversion step occurs with a graft copolymer membrane such as PDMS-*g*-PEO (the membrane of which

probably looks like a classical lipid bilayer) but are not possible for a triblock copolymer such as PEO-*b*-PDMS-*b*-PEO (adapted from classical textbooks on membranes[55]).

Another effect observed by cryo-TEM is the disappearance of the worm-like micelles upon the shock. In the classical description of the shape of self-assembled amphiphilic structures, the main parameter governing the final morphology is the relative size of hydrophilic and hydrophobic part, which determines the curvature of the hydrophilic/hydrophobic interface.[56, 57] In the present case, the simultaneous presence of vesicles and wormlike micelles under isotonic conditions indicates that the system could be locked at an intermediate value, favoring both kinds of structures. Addition of glucose may result in a small dehydration of PEO chain,[52] thus lowering the interfacial area of the hydrophilic block and decreasing the spontaneous curvature of the interface. This can explain why wormlike micelles almost disappeared in hypertonic conditions. The small membrane thickening (from 11.4 to 11.7 nm) can also be ascribed to this dehydration of the PDMS / PEO interface upon glucose addition, the contrast of dehydrated PEO being higher than that of the hydrated state.

Conclusion.

In this work, we studied the behavior of polymer vesicles at nanometric scale under osmotic stresses. Copolymers with the same hydrophobic block in a fluid state (PDMS) but different molecular weight and architecture were chosen in order to understand crucial parameters governing structural changes. On the one hand, hypotonic shocks led to a slight swelling of the nano-vesicles, as for giant polymersomes. On the other hand, hypertonic shocks led to more complex behaviors. Combination of SANS and Cryo-TEM allowed an unprecedented understanding of this complexity. It was indeed observed that water-filled PDMS-*g*-PEO unilamellar vesicles transform into bi-lamellar nested vesicles when submitted to

hypertonic conditions. This is to our knowledge the first time that the formation of such structure, known until now for liposomes only,[43] is also reported for polymersomes. The shape evolution trajectory is in agreement with theoretical predictions of the area difference elasticity model, although the membrane thickness cannot be considered negligible compared to the vesicle radius in our system. In particular, for two different types of vesicle membranes (either bilayers or monolayers obtained *via* self-assembly of respectively grafted copolymer or triblock copolymer) it was evidenced that above a critical membrane thickness/vesicle radius ratio (δ/R) of about 0.25, invaginations under hypertonic conditions are no more possible and vesicles remain unilamellar, while undergoing simply a stretching deformation. Finally, we have shown that the architecture of the copolymer plays a crucial role on the final morphology of the vesicles submitted to hypertonic shock. It was especially observed that vesicles obtained from the self-assembly of a triblock copolymer (PEO-*b*-PDMS-*b*-PEO) do not evolve further than the stomatocyte shape, the well-defined architecture of their membrane disfavoring the membrane hemifusion step needed to eventually reach a closed nested vesicle structure.

Methods.

Materials. The graft copolymer used, PDMS-*g*-PEO (Dow Corning 5329), was a gift from Dow Corning. All the molecular characterization were performed in the lab in a previous study [58] and the results were in perfect agreement with data already available in literature. [59, 60] Briefly, it is on average composed of a PDMS chain decorated with two branches of PEO, with a polymerization degree of about 12. The weight fraction of ethylene oxide is 47%. The average viscosity molecular weight is equal to 3000 g/mol and the dispersity index is 1.32 as measured by SEC. This copolymer gives birth in aqueous solutions to polymersomes whose membrane have a

core thickness of 5 nm[48] which was also checked by cryo-TEM in a previous study of our group. [58]

Deuterated glucose-d12 was purchased from Santa Cruz Biotechnology.

Synthesis of PEO-b-PDMS-b-PEO triblock amphiphilic copolymer. This copolymer was obtained by coupling two different blocks (Figure S7). Macro-initiator α,ω-bis aminopropyl terminated poly(dimethylsiloxane) with a number average molecular weight of 5000 g/mol (according to supplier data) was purchased from ABCR, Germany. α-methoxy-ω-N hydroxysuccinimide ester poly(ethylene glycol) with a number average molecular weight of 750 g/mol was purchased from Rapp polymer, Germany. This coupling reaction was done in dichloromethane at room temperature for 24 h. The success of the coupling was monitored using in ^{1}H NMR the disappearance of the NHS leaving group signal and the signal shift for carbon's proton in α position of the amine groups that turned into amide upon the reaction (Figure S8). The polydispersity index of the final triblock copolymer was evaluated to be 1.26 using SEC on 5 mg/mL polymer solution in THF and using polystyrene standard calibration curve. The triblock copolymer number average molar mass is 6800 g/mol and the hydrophilic weight fraction 22 wt.%.

Polymersome preparation. Vesicles of PDMS-*g*-PEO were spontaneously obtained by mixing the polymer with aqueous solution (distilled water for the samples used for hypertonic shocks and 1M glucose solution for the samples used for hypotonic shocks) at 10 mg/mL and stirring at 250 rpm for 2 hours. Then, in order to obtain monodisperse unilamellar vesicles, the solution was extruded 19 times through two polycarbonate membranes with a 0.1 µm pore size using a double-syringe mini-extruder (Avanti Polar Lipids, Alabaster, AL, Canada). Vesicles of PEO-*b*-PDMS-*b*-PEO were obtained from a double-emulsion – evaporation method as such: (1) 46 mg of polymer was dissolved per mL of

chloroform. (2) 0.02 mL of aqueous solution was added to 0.2 mL of polymer solution prior to 20 sec of probe sonication. (3) The entire resulting emulsion was added drop-wise to 0.9 mL of aqueous solution (the same as in step 2) and sonicated again for 2 minutes. (4) Resulting solution was extruded 19 times through two polycarbonate membranes with a 0.1 µm pore size.

Osmotic shock. Vesicles in their native state are in isotonic conditions, *i.e.* not subjected to any glucose concentration gradient and prepared at an initial concentration of 10 mg/mL. Hypertonic shocks were applied by adjusting the external concentration to the desired osmolarity using freshly prepared glucose solutions (1M for DLS and cryo-TEM experiments, 2M for SANS experiments). As vesicles were water-filled for these hypertonic shocks, the final glucose concentration gradient is the osmolarity at which the external medium was adjusted. Glucose solutions used for the SANS experiments were prepared with 75% deuterated glucose and 25% hydrogenated glucose in order to obtain the same calculated scattering length density as deuterated water. For DLS experiments, both distilled water and a 1M glucose solution were used to dilute the samples (for hypertonic and hypotonic shocks) in order to end up with the desired glucose concentration gradients and a theoretical polymer concentration of 1 mg/mL.

Instrumentation and measurements.

Nuclear Magnetic Resonance (NMR) Spectroscopy: ^{1}H NMR spectra were recorded on a Bruker Avance AC 400 spectrometer.

Size Exclusion Chromatography (SEC): A Varian apparatus was used, equipped with both refractive index and UV detectors. Analyses were performed using THF as eluent (1 mL.min^{-1}) and trichlorobenzene as flow marker.

Dynamic Light Scattering (DLS): Light scattering were carried out on a Malvern Zetasizer Nano ZS at 25° C and 90°

scattering angle (633 nm wavelength). Values of viscosity used for proper determination of the hydrodynamic radius are indicated in Figure S9.

Small Angle Neutron Scattering (SANS): These experiments were performed at the Laboratoire Léon Brillouin (CEA-CNRS, Saclay) on PACE and TPA spectrometers (respectively SANS and VSANS). Three configurations were used on the PACE spectrometer to cover scattering vectors from 2.4×10^{-3} to 3.7×10^{-1} Å^{-1}: (1) sample-to detector distance D = 4.7 m and neutron wavelength λ = 17 Å, (2) D = 3 m and λ = 6 Å, and (3) D = 1 m and λ = 6 Å. Complementary, the TPA spectrometer allows to access lower q values, here down to 10^{-3} Å^{-1} with a good resolution (D = 6 m and λ = 6 Å) up to low q values obtained with PACE spectrometer. Analyses were performed on samples of initial concentration 1 wt.% in D_2O in 2-mm-thick quartz cells.

Cryo-Transmission Electron Microscopy (cryo-TEM): 5µl of the solution were deposited onto a freshly glow discharged 400 Cu grid covered with a carbon holey film. The grid is rapidely plunged into liquid ethane cooled by liquid nitrogen by a homemade T° controlled freezing device. The grid was then mounted onto a Gatan 626 cryoholder and transferred into a FEI-Tecnai G2 cryo TEM. The grids were observed under low dose conditions and the pictures taken with an Eagle 2k2k slow scan CCD camera. Analyses were performed on samples of initial concentration 1 wt.%.

Aspect ratios were determined by fitting each vesicle by an ellipse model using the ImageJ software (http://rsb.info.nih.org/ij) and defined as the semi-minor axis (b_0) divided by the semi-major axis (a_0) of the fitting ellipse (K=b_0/a_0).

Acknowledgment. This work was supported by the Commissariat à l'énergie atomique et aux energies alternatives (CEA) and Conseil Régional d'Aquitaine for PhD funding of R. Salva (CTCR grant). ESF Research Network Programme P2M "Precision Polymer Materials" is also

acknowledged. C. Chevallard and H. Nuss are warmly thanked for participation to preliminary neutron runs.

Supporting information available. Description of the SANS models used to fit the experimental data. Additional SANS curves for PDMS-*g*-PEO and PBut-*b*-PEO vesicles under positive and negative osmotic pressure gradients. Additional cryo-TEM images with defects from the membrane fusion after hypertonic stress. Estimates of the initial radius R_0 of all vesicles. Protocol for the PEO-*b*-PDMS-*b*-PEO synthesis. Viscosities of glucose solutions for DLS measurements. This material is available free of charges *via* the Internet at http://pubs.acs.org.

References.

1. Discher, B. M.; Won, Y.-Y.; Ege, D. S.; Lee, J. C.-M.; Bates, F. S.; Discher, D. E.; Hammer, D. A. Polymersomes: Tough Vesicles Made from Diblock Copolymers. *Science* **1999,** *284*, 1143-1146.
2. Discher, D. E.; Eisenberg, A. Polymer Vesicles. *Science* **2002,** *297*, 967-973.
3. Nicolas, J.; Mura, S.; Brambilla, D.; Mackiewicz, N.; Couvreur, P. Design, Functionalization Strategies and Biomedical Applications of Targeted Biodegradable/Biocompatible Polymer-Based Nanocarriers for Drug Delivery. *Chem. Soc. Rev.* **2013,** *42*, 1147-1235.
4. Meng, F.; Zhong, Z.; Feijen, J. Stimuli-Responsive Polymersomes for Programmed Drug Delivery. *Biomacromolecules* **2009,** *10*, 197-209.
5. Renggli, K.; Baumann, P.; Langowska, K.; Onaca, O.; Bruns, N.; Meier, W. Selective and Responsive Nanoreactors. *Adv. Funct. Mater.* **2011,** *21*, 1241-1259.
6. Peters, R. J. R. W.; Louzao, I.; van Hest, J. C. M. From Polymeric Nanoreactors to Artificial Organelles. *Chem. Sci.* **2012,** *3*, 335-342.
7. Picker, A.; Nuss, H.; Guenoun, P.; Chevallard, C. Polymer Vesicles as Microreactors for Bioinspired Calcium Carbonate Precipitation. *Langmuir* **2011,** *27*, 3213-3218.
8. Marguet, M.; Bonduelle, C.; Lecommandoux, S. Multicompartmentalized Polymeric Systems: Towards Biomimetic Cellular Structure and Function. *Chem. Soc. Rev.* **2013,** *42*, 512-529.
9. Winterhalter, M.; Hilty, C.; Bezrukov, S. M.; Nardin, C.; Meier, W.; Fournier, D. Controlling Membrane Permeability with Bacterial Porins: Application to Encapsulated Enzymes. *Talanta* **2001,** *55*, 965-971.
10. Kumar, M.; Grzelakowski, M.; Zilles, J.; Clark, M.; Meier, W. Highly Permeable Polymeric Membranes Based on the Incorporation of the Functional Water Channel Protein Aquaporin Z. *Proc. Natl. Acad. Sci. U.S.A.* **2007,** *104*, 20719-20724.
11. Marguet, M.; Sandre, O.; Lecommandoux, S. Polymersomes in "Gelly" Polymersomes: Toward Structural Cell Mimicry. *Langmuir* **2012,** *28*, 2035-2043.
12. Le Meins, J. F.; Sandre, O.; Lecommandoux, S. Recent Trends in the

Tuning of Polymersomes' Membrane Properties. *Eur. Phys. J. E* **2011,** *34*, 1-17.
13. Abkarian, M.; Massiera, G.; Berry, L.; Roques, M.; Braun-Breton, C. A Novel Mechanism for Egress of Malarial Parasites from Red Blood Cells. *Blood* **2011,** *117*, 4118-4124.
14. Callan-Jones, A.; Albarran Arriagada, O. E.; Massiera, G.; Lorman, V.; Abkarian, M. Red Blood Cell Membrane Dynamics During Malaria Parasite Egress. *Biophys. J.* **2012,** *103*, 2475-2483.
15. Perrault, S. D.; Walkey, C.; Jennings, T.; Fischer, H. C.; Chan, W. C. W. Mediating Tumor Targeting Efficiency of Nanoparticles Through Design. *Nano Lett.* **2009,** *9*, 1909-1915.
16. Chithrani, B. D.; Ghazani, A. A.; Chan, W. C. W. Determining the Size and Shape Dependence of Gold Nanoparticle Uptake into Mammalian Cells. *Nano Lett.* **2006,** *6*, 662-668.
17. Chauhan, V. P.; Popović, Z.; Chen, O.; Cui, J.; Fukumura, D.; Bawendi, M. G.; Jain, R. K. Fluorescent Nanorods and Nanospheres for Real-Time In Vivo Probing of Nanoparticle Shape-Dependent Tumor Penetration. *Angew. Chem. Int. Ed.* **2011,** *50*, 11417-11420.
18. Champion, J. A.; Katare, Y. K.; Mitragotri, S. Particle Shape: A New Design Parameter for Micro- and Nanoscale Drug Delivery Carriers. *J. Controlled Release* **2007,** *121*, 3-9.
19. Decuzzi, P.; Pasqualini, R.; Arap, W.; Ferrari, M. Intravascular Delivery of Particulate Systems: Does Geometry Really Matter? *Pharm. Res.* **2009,** *26*, 235-243.
20. Sharma, G.; Valenta, D. T.; Altman, Y.; Harvey, S.; Xie, H.; Mitragotri, S.; Smith, J. W. Polymer Particle Shape Independently Influences Binding and Internalization by Macrophages. *J. Controlled Release* **2010,** *147*, 408-412.
21. Boucher, P.-A.; Morris, C. E.; Joós, B. Mechanosensitive Closed-Closed Transitions in Large Membrane Proteins: Osmoprotection and Tension Damping. *Biophys. J.* **2009,** *97*, 2761-2770.
22. Howard, R. J.; Ferrari, M. A.; Roach, D. H.; Money, N. P. Penetration of Hard Substrates by a Fungus Employing Enormous Turgor Pressures. *Proc. Natl. Acad. Sci. U.S.A.* **1991,** *88*, 11281-11284.
23. Battaglia, G.; Ryan, A. J.; Tomas, S. Polymeric Vesicle Permeability: A Facile Chemical Assay. *Langmuir* **2006,** *22*, 4910-4913.
24. Boroske, E.; Elwenspoek, M.; Helfrich, W. Osmotic Shrinkage of Giant Egg-Lecithin Vesicles. *Biophys. J.* **1981,** *34*, 95-109.
25. Li, W.; Aurora, T. S.; Haines, T. H.; Cummins, H. Z. Elasticity of Synthetic Phospholipid Vesicles and Submitochondrial Particles During Osmotic Swelling. *Biochemistry* **1986,** *25*, 8220-8229.
26. Carlsen, A.; Glaser, N.; Le Meins, J.-F.; Lecommandoux, S. Block Copolymer Vesicle Permeability Measured by Osmotic Swelling and Shrinking. *Langmuir* **2011,** *27*, 4884-4890.
27. Shum, H. C.; Kim, J.-W.; Weitz, D. A. Microfluidic Fabrication of Monodisperse Biocompatible and Biodegradable Polymersomes with Controlled Permeability. *J. Am. Chem. Soc.* **2008,** *130*, 9543-9549.
28. Käs, J.; Sackmann, E. Shape Transitions and Shape Stability of Giant Phospholipid Vesicles in Pure Water Induced by Area-to-Volume Changes. *Biophys. J.* **1991,** *60*, 825-844.
29. Seifert, U. Configurations of Fluid Membranes and Vesicles. *Adv. Phys.* **1997,** *46*, 13-137.
30. Wintz, W.; Döbereiner, H.-G.; Seifert, U. Starfish Vesicles. *Europhys. Lett.* **1996,** *33*, 403-408.
31. Michalet, X. Equilibrium Shape Degeneracy in Starfish Vesicles. *Phys. Rev. E* **2007,** *76*, 021914.
32. Ménager, C.; Cabuil, V. Reversible Shrinkage of Giant Magnetoliposomes under an Osmotic Stress. *J. Phys. Chem. B* **2002,** *106*, 7913-7918.
33. Claessens, M. M. A. E.; Leermakers, F. A. M.; Hoekstra, F. A.;

Stuart, M. A. C. Osmotic Shrinkage and Reswelling of Giant Vesicles Composed of Dioleoylphosphatidylglycerol and Cholesterol. *Biochim. Biophys. Acta* **2008,** *1778*, 890-895.
34. Bernard, A.-L.; Guedeau-Boudeville, M.-A.; Jullien, L.; di Meglio, J.-M. Raspberry Vesicles. *Biochim. Biophys. Acta* **2002,** *1567*, 1-5.
35. Bealle, G.; Jestin, J.; Carriere, D. Osmotically Induced Deformation of Capsid-Like Icosahedral Vesicles. *Soft Matter* **2011,** *7*, 1084-1089.
36. Li, X.; Pivkin, I. V.; Liang, H.; Karniadakis, G. E. Shape Transformations of Membrane Vesicles from Amphiphilic Triblock Copolymers: A Dissipative Particle Dynamics Simulation Study. *Macromolecules* **2009,** *42*, 3195-3200.
37. Yuan, H.; Huang, C.; Zhang, S. Dynamic Shape Transformations of Fluid Vesicles. *Soft Matter* **2010,** *6*, 4571-4579.
38. Lorenceau, E.; Utada, A. S.; Link, D. R.; Cristobal, G.; Joanicot, M.; Weitz, D. A. Generation of Polymerosomes from Double-Emulsions. *Langmuir* **2005,** *21*, 9183-9186.
39. Pencer, J.; White, G. F.; Hallett, F. R. Osmotically Induced Shape Changes of Large Unilamellar Vesicles Measured by Dynamic Light Scattering. *Biophys. J.* **2001,** *81*, 2716-2728.
40. Beney, L.; Linares, E.; Ferret, E.; Gervais, P. Influence of the Shape of Phospholipid Vesicles on the Measurement of Their Size by Photon Correlation Spectroscopy. *Eur. Biophys. J.* **1998,** *27*, 567-574.
41. Hubert, D. H. W.; Jung, M.; Frederik, P. M.; Bomans, P. H. H.; Meuldijk, J.; German, A. L. Morphology Transformations of DODAB Vesicles Reminiscent of Endocytosis and Vesicular Traffic. *Langmuir* **2000,** *16*, 8973-8979.
42. Saveyn, P.; Cocquyt, J.; Bomans, P.; Frederik, P.; De Cuyper, M.; Van der Meeren, P. Osmotically Induced Morphological Changes of Extruded Dioctadecyldimethylammonium Chloride (DODAC) Dispersions. *Langmuir* **2007,** *23*, 4775-4781.
43. Pitard, B.; Oudrhiri, N.; Lambert, O.; Vivien, E.; Masson, C.; Wetzer, B.; Hauchecorne, M.; Scherman, D.; Rigaud, J.-L.; Vigneron, J.-P., *et al.* Sterically Stabilized BGTC-Based Lipoplexes: Structural Features and Gene Transfection into the Mouse Airways *in Vivo*. *J. Gene Med.* **2001,** *3*, 478-487.
44. Kim, K. T.; Zhu, J.; Meeuwissen, S. A.; Cornelissen, J. J. L. M.; Pochan, D. J.; Nolte, R. J. M.; van Hest, J. C. M. Polymersome Stomatocytes: Controlled Shape Transformation in Polymer Vesicles. *J. Am. Chem. Soc.* **2010,** *132*, 12522-12524.
45. Azzam, T.; Eisenberg, A. Fully Collapsed (Kippah) Vesicles: Preparation and Characterization. *Langmuir* **2010,** *26*, 10513-10523.
46. Meeuwissen, S. A.; Kim, K. T.; Chen, Y.; Pochan, D. J.; van Hest, J. C. M. Controlled Shape Transformation of Polymersome Stomatocytes. *Angew. Chem. Int. Ed.* **2011,** *50*, 7070-7073.
47. Mui, B. L.-S.; Cullis, P. R.; Evans, E. A.; Madden, T. D. Osmotic Properties of Large Unilamellar Vesicles Prepared by Extrusion. *Biophys. J.* **1993,** *64*, 443-453.
48. Lin, Z.; Hill, R. M.; Davis, H. T.; Scriven, L. E.; Talmon, Y. Cryo Transmission Electron Microscopy Study of Vesicles and Micelles in Siloxane Surfactant Aqueous Solutions. *Langmuir* **1994,** *10*, 1008-1011.
49. Pedersen, J. S. Analysis of Small-Angle Scattering Data from Colloids and Polymer Solutions: Modeling and Least-Squares Fitting. *Adv. Colloid Interface Sci.* **1997,** *70*, 171-210.
50. Kahraman, O.; Stoop, N.; Müller, M. M. Fluid Membrane Vesicles in Confinement. *New J. Phys.* **2012,** *14*, 095021.
51. Kahraman, O.; Stoop, N.; Müller, M. M. Morphogenesis of Membrane Invaginations in Spherical Confinement. *EPL* **2012,** *97*, 68008.
52. Sarkar, B.; Ravi, V.; Alexandridis, P. Micellization of Amphiphilic Block

Copolymers in Binary and Ternary Solvent Mixtures. *J. Colloid Interface Sci.* **2013,** *390*, 137-146.
53. Nardin, C.; Winterhalter, M.; Meier, W. Giant Free-Standing ABA Triblock Copolymer Membranes. *Langmuir* **2000,** *16*, 7708-7712.
54. Helfrich, W.; Servuss, R. M. Undulations, Steric Interaction and Cohesion of Fluid Membranes. *Il Nuovo Cimento D* **1984,** *3*, 137-151.
55. Arnold, K. Cation-Induced Vesicle Fusion Modulated by Polymers and Proteins. In *Structure and dynamics of membranes: Generic and specific interactions*, Lipowsky, R.; Sackmann, E., Eds. Elsevier: Amsterdam, 1995; pp 903-957
56. Israelachvili, J. *Intermolecular and Surface Forces, Second Edition: With Applications to Colloidal and Biological Systems (Colloid Science)*. Academic Press: 1992.
57. Discher, D. E.; Ahmed, F. Polymersomes. *Annu. Rev. Biomed. Eng.* **2006,** *8*, 323-341.
58. Chemin, M.; Brun, P. M.; Lecommandoux, S.; Sandre, O.; Le Meins, J. F. Hybrid Polymer/Lipid Vesicles: Fine Control of the Lipid and Polymer Distribution in the Binary Membrane. *Soft Matter* **2012,** *8*, 2867-2874.
59. Hill, R. M.; He, M.; Lin, Z.; Davis, H. T.; Scriven, L. E. Lyotropic Liquid Crystal Phase Behavior of Polymeric Siloxane Surfactants. *Langmuir* **1993,** *9*, 2789-2798.
60. Nam, J.; Santore, M. M. Adhesion Plaque Formation Dynamics between Polymer Vesicles in the Limit of Highly Concentrated Binding Sites. *Langmuir* **2007,** *23*, 7216-7224.

Supporting Information for:

Polymersomes Shape Transformation at the Nanoscale

Romain Salva,[†,‡] Jean-François Le Meins,[†] Olivier Sandre,[†] Annie Brûlet,[§] Marc Schmutz,[⊥] Patrick Guenoun,[,‡] and Sébastien Lecommandoux [*,†]*

[†]Université de Bordeaux/IPB, ENSCBP, 16 avenue Pey-Berland, 33607 Pessac, France, LCPO, UMR 5629, Pessac, France

[‡]IRAMIS, LIONS, UMR SIS2M 3299 CEA-CNRS, CEA Saclay, F-91191 Gif-sur-Yvette Cedex, France

[§]Laboratoire Léon Brillouin, LLB, UMR12, CNRS-CEA Saclay, F-91191 Gif-sur-Yvette Cedex, France

[⊥]Institut Charles Sadron, UPR 22 CNRS, Université de Strasbourg, 23 rue du Loess, 67034 Strasbourg, France

Small angle neutron scattering – Raw intensity curves. The SANS curves are presented for vesicles made of $PDMS_{22}$-*g*-PEO_{12} (Dow Corning) in various hypertonic and hypotonic conditions. All measurements were performed in 5 mm-thick quartz cells. The isotonic samples (0/0 and 1000 mM/1000 mM glucose in D_2O) had a concentration of 10 mg/mL. The hypertonic samples were almost as concentrated as the initial ones (*e.g.* 9.75 g/L for the 0/100mM samples). The hypotonic samples had a lower weight concentration due to

dilution by pure D_2O (*e.g.* 7.5 g/L for the 1000 mM/750 mM samples). The SANS profiles plotted on Figure S1 are normalized by the polymer concentration.

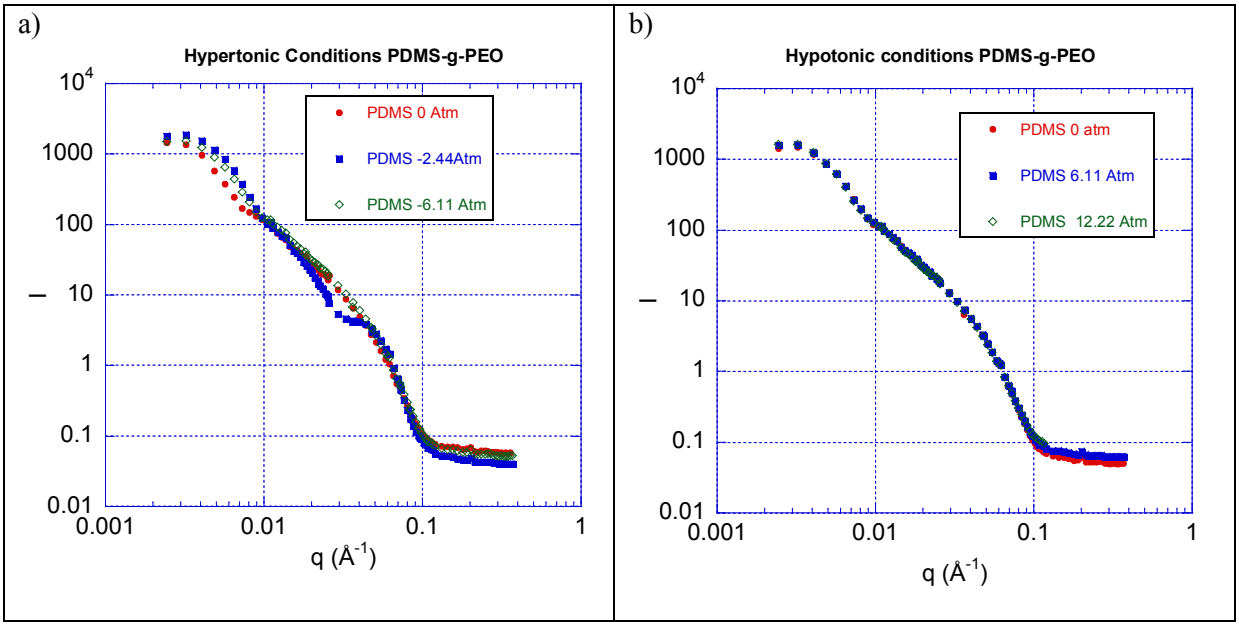

Figure S1. SANS curves for PDMS-g-PEO vesicles in hypertonic conditions (a) and hypotonic conditions (b).

It is clear than in hypertonic conditions (Fig. S1a), PDMS-*g*-PEO polymersomes undergo modifications, presumably the formation of nested vesicles, whereas they do not change in hypotonic conditions (Fig. S1b). This is an interesting result of the SANS study as it is similar to direct observations of PDMS-*g*-PEO giant vesicles, for which the invariance of the vesicle size in hypotonic condition was attributed to a fast swell burst cycle.[16]

We evaluated the radii of gyration of the vesicles in the Guinier (low q) regime and their membrane thicknesses using the Kratky-Porod approximation in the intermediate q regime ($\mathrm{Ln}I\times q^2$ varying like $-q^2H^2/12$). In hypertonic conditions, we observed a slight decrease of the radius of gyration (from 43 nm to 35 nm). The membrane thicknesses H deduced by Kratky-Porod plots seems to be unchanged for PDMS-g-PEO (~6.4 nm). In hypotonic conditions, the radius of gyration and membrane thickness remain unchanged.

Small angle neutron scattering - Multi Shell Form Factor. The experimental data of small angle neutrons scattering for PDMS-*g*-PEO vesicles in hypertonic conditions have been fitted using a multi shell form factor. It corresponds to two spherical shells of same center separated by a layer of solvent. As cryo-TEM experiments evidenced, thicknesses and scattering length densities (SLD) of the internal and external shells are identical: $\delta_i = \delta_e = \delta_{shell}$ and $\rho_i = \rho_e = \rho_{shell}$.

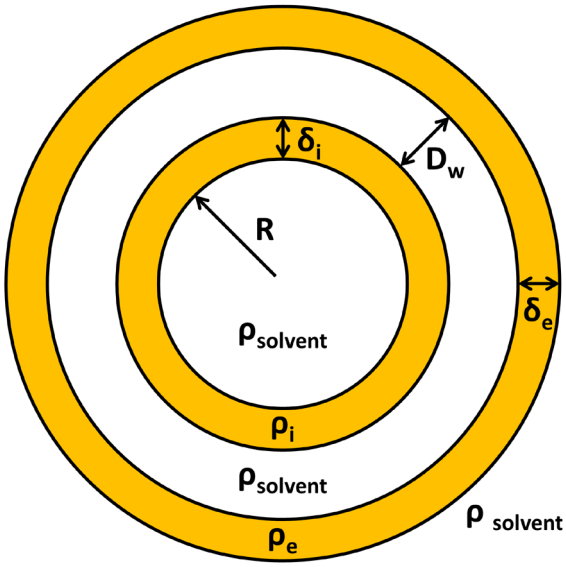

Figure S2. Multi-Shell Model.

Scattering length densities used to fit the experimental curves were $\rho_{shell} = \rho_{PDMS} = 6.37\times10^{-8}$ Å^{-2} and $\rho_{solvent} = \rho_{D2O} = 6.35\times10^{-6}$ Å^{-2}.

Using this model assumes that the PEO layers covering the PDMS shells are almost fully hydrated and have no contrast with the deuterated water ($\Delta\rho^2 = (\rho_{hydrated\ PEO} - \rho_{D2O})^2 \sim 0$).

Defects from the membrane fusion for PDMS-g-PEO vesicles. Two different kinds of defects results from the membrane fusion to close stomatocytes and reach a nested structure. Most of the time, a “round mark” is present in the internal cavity of the nested vesicle. We assume that these marks are membrane buds of the inner shell because they can

be seen in all space direction and the structures are always closed. It was attributed to an excess of surface membrane area of the inner shell when the membrane of stomatocytes fused, due to the small size of the initial vesicles. Indeed, the curvature of the edges of the stomatocyte opening was not negligible compared to the vesicle radius.

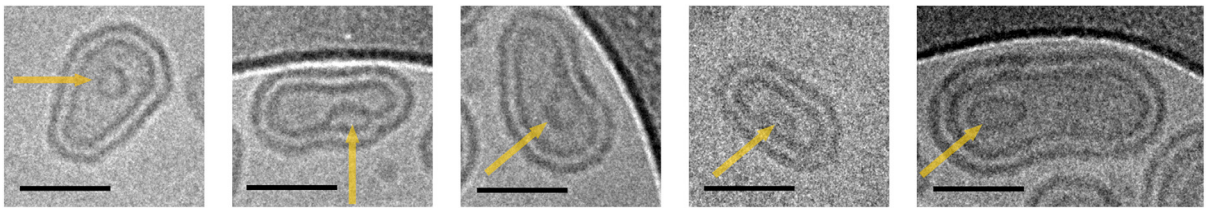

Figure S3. Cryo-TEM images of PDMS-*g*-PEO nested vesicles with the internal buds (showed by arrows) resulting from the membrane fusion and budding. Scale bars represent 50 nm.

Additionally, "scars" in the membrane can also be seen on some vesicles and show the location in membrane area where the fusion most likely took place. On cryo-TEM images, it was seen as a darken area in the double membrane. It can be noted that the internal bud was not localized in the same region as this scar.

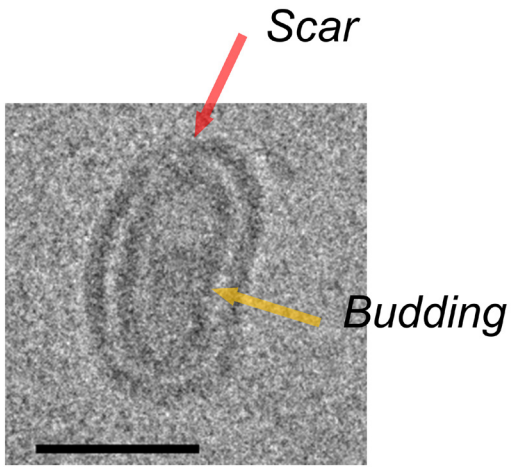

Figure S4. Cryo-TEM images of a nested vesicle with a "scar" in the bi-lamellar membrane resulting from the fusion of the two edges of a stomatocyte. Scale bar represents 50 nm.

Estimate of the initial radius R_0 of the vesicles. All vesicles, unilamellar and nested, were fitted by an ellipse using the ImageJ software. It gave the values of the semi-major axis a_0 and semi-minor axis b_0 for the external shell. With the assumption that all vesicles are prolate ellipsoids, the surface membrane area of the external shell can be calculated using following equation:

$$A_{prolate} = 2\pi {b_0}^2 + \frac{2\pi a_0 b_0}{e_0} Arcsin(e_0) \text{ with } e_0 = \frac{\sqrt{{a_0}^2 - {b_0}^2}}{a_0}$$

For nested vesicles, the total surface membrane area also includes the surface of the internal vesicles, with a semi-major axis $a_1 = a_0 - (\delta + D_w)$ and a semi-minor axis $b_1 = b_0 - (\delta + D_w)$. Parameters δ and D_w are respectively the membrane thickness and the water gap between the shells.

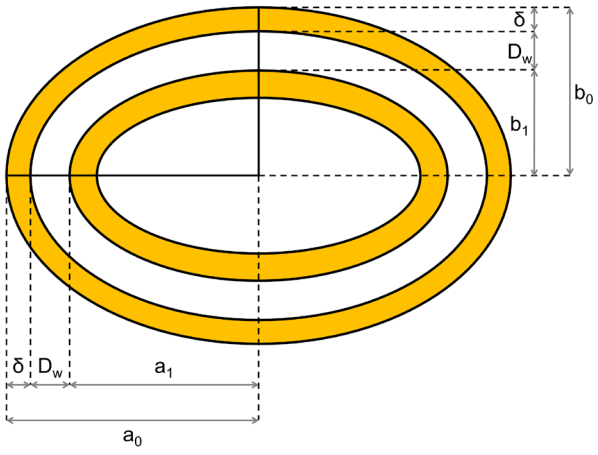

Figure S5. Scheme of the characteristics sizes of a nested vesicle.

As the surface of a sphere is $A = 4\pi R^2$, we can calculate the initial radius R_0 of the sphere: $R_0 = \sqrt{\frac{A}{4\pi}} = \sqrt{\frac{\sum_i \left(2\pi {b_i}^2 + \frac{2\pi a_i b_i}{e_i} Arcsin(e_i)\right)}{4\pi}} = \left[\sum_i \left(\frac{{b_i}^2}{2} + \frac{a_i b_i}{2e_i} Arcsin(e_i)\right)\right]^{\frac{1}{2}}$

Small angle neutron scattering - Core Multi-Shell Form Factor. The experimental data of small angle neutrons scattering for PEO-*b*-PDMS-*b*-PEO vesicles in isotonic and hypertonic conditions have been fitted using a core multi shell form factor. This model corresponds to the multi shell form factor without conditions on the different shells (different thicknesses and scattering length densities).

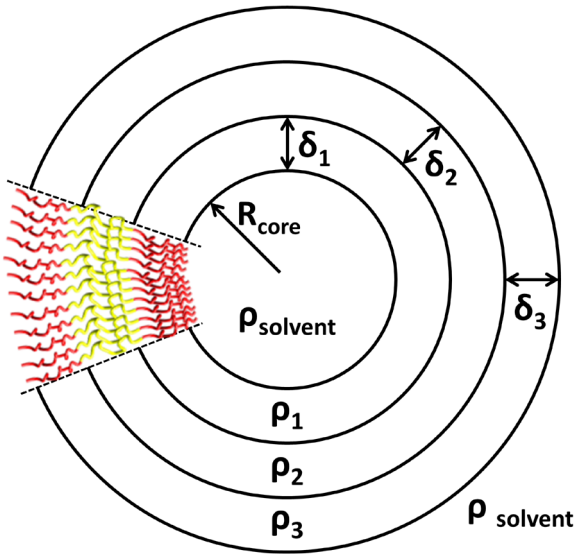

Figure S6. Core Multi Shell Model.

Conditions on scattering length densities used to fit the experimental curves were $\rho_2 = \rho_{shell} = \rho_{PDMS} = 6.37\times10^{-8}$ Å^{-2} and $\rho_{solvent} = 6.35\times10^{-6}$ Å^{-2} > ρ_1 and ρ_3 > $\rho_{dehydrated\ PEO} = 5.69\times10^{-7}$ Å^{-2}.

As explained in the model previously described, PEO layers cannot be seen in these SANS experiments if they are totally hydrated. Then, shells 1 and 3 do not represent the entire PEO layers covering the PDMS shell but only the part of PEO chains close to the PDMS / PEO

interface, where they are not well hydrated. It can be represented as a SLD gradient along PEO chains. The total membrane thickness is $\delta = \delta_1 + \delta_2 + \delta_3$.

Table SI-1. Membrane parameters determined for PEO-*b*-PDMS-*b*-PEO vesicles with the Core Multi Shell Model.

Δc	δ_1 (Å)	ρ_1 (Å^{-2})	δ_2 (Å)	ρ_2 (Å^{-2})	δ_3 (Å)	ρ_3 (Å^{-2})
0 mM	10.0	1.8×10^{-6}	85.6	6.37×10^{-8}	18.7	8.1×10^{-7}
250 mM	15.3	1.2×10^{-6}	90.9	6.37×10^{-8}	11.0	7.4×10^{-7}
750 mM	18.1	1.2×10^{-6}	88.7	6.37×10^{-8}	17.8	5.69×10^{-7}

The glucose concentration gradients used for the hypertonic shocks are indicated in absolute values and correspond to the osmolarity of the external solution as vesicles were water-filled. SLD values obtained by fitting the curves are close to that of dehydrated PEO chains, and are not negligible. Indeed, the contrast with deuterated water is (for the highest value): $\Delta\rho^2 = (1.8\times10^{-6} - 6.35\times10^{-6})^2 = (4.55\times10^{-6})^2 = 2.07\times10^{-11}$ Å^{-4} → at least 52% of the PDMS layer contrast.

PEO-b-PDMS-b-PEO synthesis. This copolymer was obtained by coupling two different blocks : α,ω-bis aminopropyl terminated poly(dimethylsiloxane) as hydrophobic block (average molecular weight 5000 g/mol) and α-methoxy-ω-N hydroxysuccinimide ester poly(ethylene glycol) with a number average molecular weight of 750g/mol.

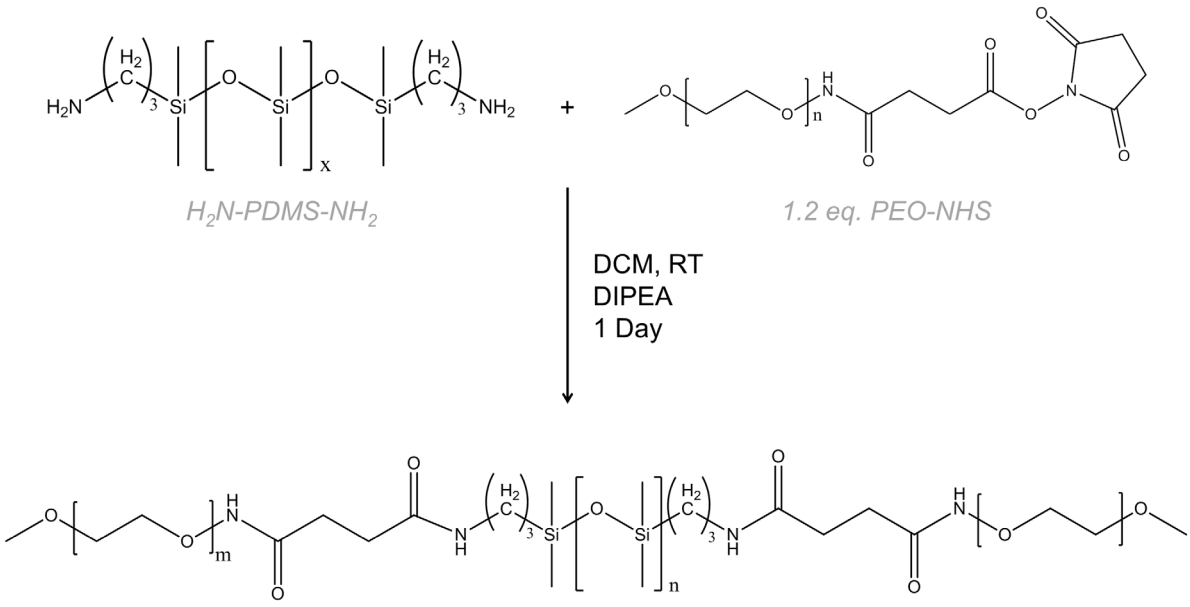

Figure S7. Coupling reaction of H_2N-PDMS-NH_2 and PEO-NHS blocks to obtain PEO-*b*-PDMS-*b*-PEO triblock copolymer.

Chain-end functionalization rate (t_{fonc}) was determined by ^{1}H NMR using the integration ratio of the PDMS main chain signal ($Si(CH_3)_2O$, $(6\times DP_{PDMS})H$, δ = 0 ppm) and the proton from the carbon in α position of the amine groups ($H_2NCH_2CH_2$, $(4\times t_{fonc})H$, δ = 2.6ppm) for the diaminated PDMS; the integration ratio of the PEO main chain signal (CH_2CH_2O, $(4\times DP_{PEO})H$, δ = 3.6 ppm) and of the leaving NHS group signal ($C(O)CH_2CH_2C(O)$, $(4\times t_{fonc})H$, δ = 2.6ppm) were used for PEO-NHS. Obtained values are 95% for the PDMS macro-initiator and 97% for PEO-NHS. Both reagents were dissolved in cryo-distilled dichloromethane, and N,N-diisopropylethylamine was added into the PEO-NHS solution to ensure that primary amine from the macro-initiator were deprotonated during the coupling reaction. Then, solutions of reactants were mixed and stirred at room temperature for 24 h. The solvent was removed under nitrogen stream, and the copolymer was dispersed in distilled water, dialyzed during 3 days (MWCO = 50 kDa), and lyophilized.

The success of the coupling between PEO-NHS and H_2N-PDMS-NH_2 macro-initiator was monitored using ^{1}H NMR. Before coupling, the signal for carbon's proton at the chain end of the macro-initiator corresponds to amine groups ($H_2NCH_2CH_2$, δ = 2.6ppm). After coupling, this signal is significantly shifted and corresponds to amide groups ($RCONHCH_2CH_2$, δ = 3.1ppm), attesting that all chain end functions reacted with PEO-NHS. Disappearance of proton signal from the NHS leaving group of PEO-NHS reactants confirms the success of the reaction and of the dialysis (to remove all unreacted products).

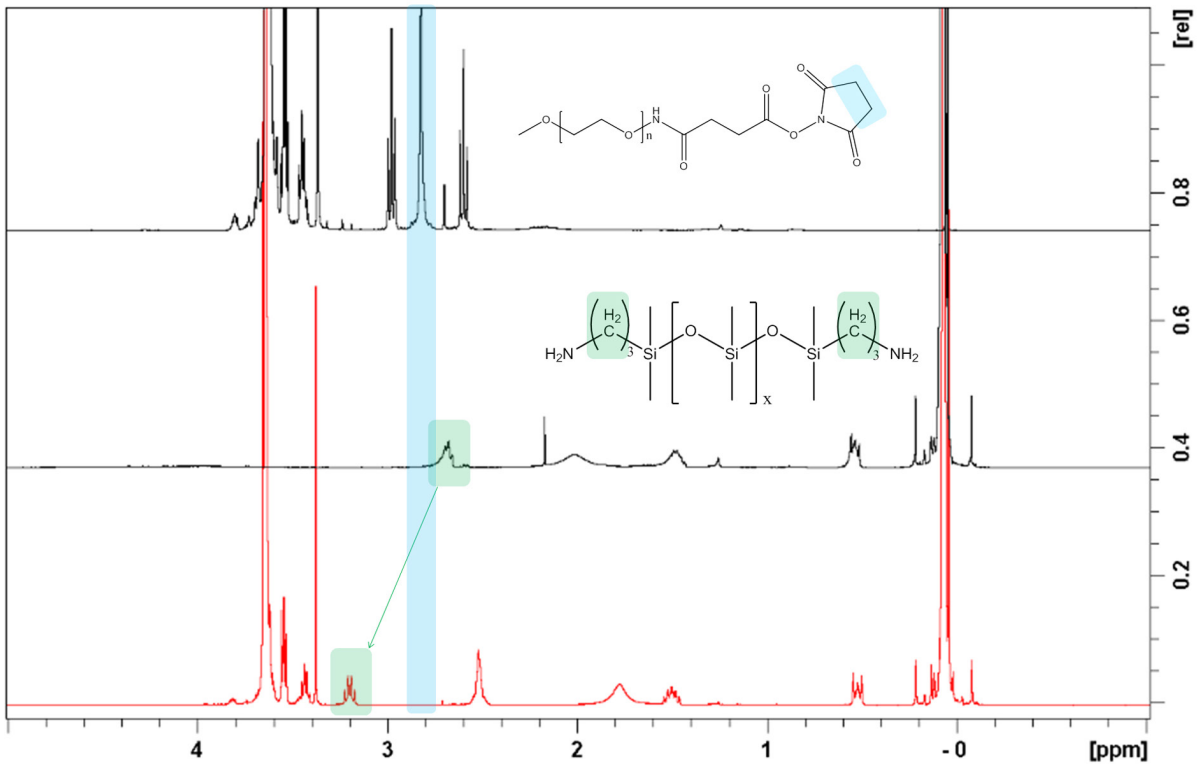

Figure S8. ^{1}H NMR spectrum in CDCl3 for PEO-NHS blocks (upper curve), H_2N-PDMS-NH_2 (middle curve) and PEO-*b*-PDMS-*b*-PEO triblock copolymer (lower curve).

Hydrodynamic radius measurements by Dynamic Light Scattering. The proper solution viscosities used for the hydrodynamic radius measurements were determined thank to a 2nd order polynomial fit of viscosity measurements carried out on glucose solutions.

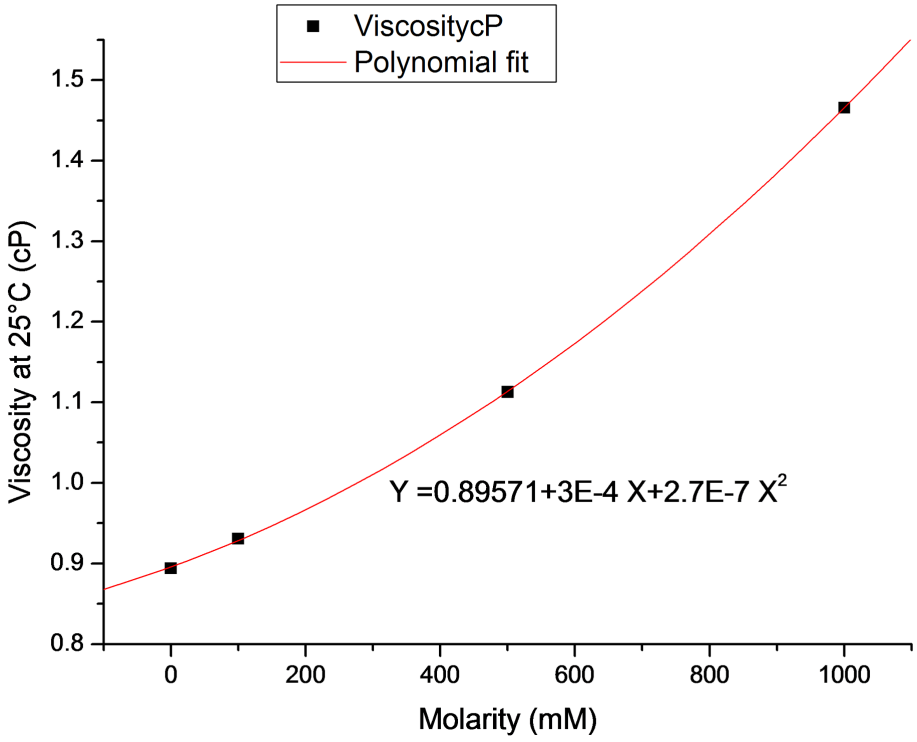

Figure S9. Viscosity of glucose solutions of varying molarity (0, 0.1, 0.5, 1) based on flow times through a Ubbelohde capillary viscometer, measured at 25°C.